Materials Characterization 189 (2022) 111942

Contents lists available at ScienceDirect

Materials Characterization

journal homepage: www.elsevier.com/locate/matchar

Facilitating the occurrence of dynamic recrystallization in plain extra low-carbon steel by warm asymmetric rolling

Satyaveer Singh Dhinwal [a,b,c,*], Clément Ernould [b,c], Benoît Beausir [b,c]

[a] Institue Jean Lamour (IJL) Campus Artem, Université de Lorraine, Nancy 54001, France
[b] Université de Lorraine, CNRS, Arts et Métiers ParisTech, LEM3, F-57070 Metz, France
[c] Laboratory of EXcellence Design of Alloy Metals for low-mAss Structure (Labex-DAMAS), Université de Lorraine, Metz 57070, France

ARTICLE INFO

Keywords:
Steel
High strain single pass
Asymmetric rolling
Dynamic recrystallization
Crystallographic textures
HR-TKD

ABSTRACT

The occurrence of dynamic recrystallization in warm rolling of plain extra-low carbon steel was examined by applying 75% thickness reduction in a single pass. The investigated temperature range was ambient to 700 °C. Results show apparently dynamic recrystallization remains absent in symmetric rolling below 600 °C. Nevertheless, dynamic recrystallization not only just occurs but accelerates as the condition of warm rolling changed from symmetric to asymmetric condition. The analysis of grain internal disorientations and geometrically necessary dislocation densities by High-angular Resolution on-axis Transmission Kikuchi Diffraction (HR-TKD) allowed to identify the type of dynamic recrystallization and its evolution through the warm temperature range. New grains formed by either continuous or discontinuous dynamic recrystallization are preferentially orientated according a typical shear texture up to 600 °C in the case of asymmetric rolling. Above 600 °C, dynamically recrystallized grains produce restrengthening in the rolling texture as well as in the overall texture.

1. Introduction

The significance of dynamic recrystallization in materials can be understood by knowing that, back in mid-1990s one of the publications by Jonas was titled “Dynamic recrystallization - scientific curiosity or industrial tool ?” [1]. The investigations on this topic are still trending with new alloys development like high entropy alloys [2–4]. In general, dynamic recrystallization is defined as a type of recrystallization process which occurs in materials under the state of stress and temperature. The knowledge of its relatively predictable way with respect to temperature makes geologists to understand crystal growth in rocks. However, metallurgists apply it to understand flow stress behavior and equiaxed grain formation in thermomechanical processing of metals. Among different metal forming methods, rolling is one of the thermomechanical processes which is in use invariably for the flat metal sheet production. Based on applied temperature to a metal, rolling can be termed as hot, warm, cold and cryo-rolling.

The occurrence of dynamic recrystallization has been investigated numerously therefore only some salient publications are referenced here especially in hot rolling of steels [5–21]. Based on the time interval between the rolling passes, dynamic recrystallization further termed as metadynamic or post dynamic recrystallization [1,6,13,19,21]. In fact, dynamic recrystallization which occurs in hot rolling is by nature of discontinuous type which means, nucleation of fine grains first and then their growing stage. There is also a so-called geometric dynamic recrystallization, which occurs at high temperature by intersection of serrated grain boundaries and get pinched off into small equiaxed grains [11,13,21–23]. The term dynamic recrystallization which was used earlier for the condition of applied stress at elevated temperature is extended to the equiaxed grain formation when severe plastic deformation is applied [11,13]. In this case, the conversion of original grains, first into sub-grains delimited by low angle boundaries and then later by high angle boundaries is a continuous process with accumulation of strain, thus, it is called continuous dynamic recrystallization.

In the literature, efforts were put to reduce hot rolling temperature to exploit the occurrence of the dynamic recrystallization. The idea was to exploit the lower temperature range of austenitic phase (A_{r3}) and upper warm temperature range of ferrite phase (A_{r1}) to conduct rolling for austenitic, micro alloyed and also for the ferritic steels. The ferritic steels like plain extra (~0.03 pct. C) to ultra-low (~0.003 pct. C) carbon grades are very low-carbon content steel. Earlier days, it was a perception that these grades of ferritic steel would show extended dynamic recovery rather than the dynamic recrystallization. By mid 1990s, it was reported that dynamic recrystallization could also occur in these grades

* Corresponding author at: Institue Jean Lamour (IJL) Campus Artem, Université de Lorraine, 54 001 Nancy, France.
E-mail address: satyaveer.dhinwal@univ-lorraine.fr (S.S. Dhinwal).

https://doi.org/10.1016/j.matchar.2022.111942
Received 18 October 2021; Received in revised form 9 April 2022; Accepted 2 May 2022
Available online 8 May 2022
1044-5803/

of steels when temperature is around lower austenitic range (A_{r3}) or in upper warm temperature of ferrite region (A_{r1}) [24–26]. The applied strain was about $\varepsilon = 1$ or above either by plain strain compression test or by a single pass of rolling (50% or above thickness reduction). Nevertheless, in lower temperature warm rolling (600 °C or below), extended dynamic recovery was reported in ferritic steels [27–36]. Although, it was also reported that ultra-low carbon steel having initial grain size of 0.5 μm showed occurrence of dynamic recrystallization at 450 °C when strain of 4 applied with slow strain rate 0.01 s^{-1} in anvil compression test [37]. Nevertheless, only dynamically recovered and elongated grains were observed when the same test was repeated for an increased strain rate equal to 1 s^{-1} [37]. In addition, when experiment was examined for an initial grain size of 200 μm, the absence of dynamic recrystallization was observed for both strain rate of 0.01 s^{-1} and 1 s^{-1} at strain of 4 [38]. Practically, the condition of high strain of 4 or above and slow strain rate of 0.01 s^{-1} is not applicable in a single pass of rolling. Also, there are no other report showing dynamic recrystallization at such lower warm temperature on ferritic steel with average grain size of ~40–80 μm produced commercially. It seems that the dynamic recrystallization observed at 450 °C is specific to ultra-fine (0.5 μm) grained ultra-low carbon steel tested at slow strain rate (0.01 s^{-1}) and high strain of 4. Therefore, prevailed dynamic recovery,which yields to softened grains, can be still anticipated in a warm rolled ferritic steels at 600 °C and below.

Recently, in a comprehensive review on dynamic recrystallization, it was mentioned that there was a lack of experimental evidences to show how dynamic recrystallization can be affected by the strain path and its concurrently evolving texture or vice versa [13]. Indeed, reports on this topic are lacking in the literature, when it is known that the different strain paths are possible in processes like rolling, extrusion or forging. Interestingly, in one report, strain path change test was carried out in torsion test [39]. It was noted that when ultra-low carbon steel is subjected to a cyclic mode of torsion at 950 °C, dynamic recovery occurs to restore the material with mild grain refinement. Nevertheless, dynamic recrystallization and severe grain refinement were observed in the monotonic mode [39].

After reviewing the literature about prevailed dynamic recovery in lower temperature warm rolling (600 °C and below) of ferritic steels and finding lack of investigations about the effect of strain path, this study attempts to carry out experiments in this direction. A single pass rolling conducted with similar parameters and grain size as used in literature of warm rolling of ferritic steel especially on extra to ultra-low carbon steels [33,40]. Strain path change in multi-pass rolling can be imposed by changing the rolling direction in each successive pass. However, only a rotation of 90° of the sheet around the normal direction in alternate pass, also termed as cross rolling, can have profound change in texture, thus, a strong possibility to influence dynamic recrystallization [41–44]. There is also another method to provide strain path change by 180° rotation along all three major directions of a specimen when asymmetric condition imposed in multi-pass rolling [45]. The strain path change in asymmetric rolling can impose shear strain reinforcement and its reversion depending on the path selection [45,46]. The texture, microstructure and grain boundary characteristics are very sensitive to the strain path selection in asymmetric rolling [45]. However, it is also important to note that the selection of processing parameters play a vital role in the effectiveness of shear strain [45–47].

In literature of steel, it was noted that the asymmetric rolling carried out either in ambient or in hot condition[45–57]. It was mostly due to having prime focus on the evolution of texture, microstructure, phase transformation and mechanical properties et cetera. The warm temperature range between ambient and below -austenite -to -ferrite phase transformation temperature of steels has not been investigated in the asymmetric rolling. Except for an investigation about the twinning activities and texture evolution in high manganese Twinning induced Plasticity (TWIP) steel [57]. Therefore, a complete lack of evidence about how warm rolling under imposed asymmetry will affect the microstructure evolution of extra-low carbon grade of ferritic steels, thus, the dynamic recrystallization and its type. As, it was mentioned earlier, the discontinuous dynamic recrystallization in extra-low carbon grade of ferritic steel has been the subject of matter to find ways to observe and extend its formation in conventional rolling below austenite to ferrite phase transformation (especially below 700 °C). For this reason, present investigation is on plain extra-low carbon steel where change in roll diameters ratio applied as an imposed asymmetry to compare with symmetric rolling, thus the interference of shear on rolling strain in a single pass of rolling. The additional investigation related to multi-pass warm asymmetric rolling, where strain path change along three directions of the specimen can be taken in account, has been refrained in present study and left for the future work.

2. Experimental methodology

2.1. Rolling

The plain extra-low carbon steel of 0.03C-0.15Mn-0.006Si-0.001Ti (weight percentage) was heat treated at 1050 °C for an hour and air-cooled subsequently. This step was taken in order to homogenize the microstructure and weaken the initial texture. From this heat-treated slab, the specimens with dimensions of 30 mm width × 60 mm length and 5 mm in thickness were machined. The front end of specimens was wedged to facilitate ease in the roll bite. Rolling mill was equipped with four set of roll diameters ratio 1:1, 1:1.3, 1:1.6 and 1:2. These set of rolls were adjacent to each other and co-axially positioned on the two shafts of a single motor driven rolling mill. By this way, a comparative investigation can be made easily between symmetric case and other three different set of roll diameters ratios for a given thickness reduction per pass. The roll setup design used for the present investigation can be find in ref. [52]. A single pass of 70–75% thickness reduction was aimed on a very thinly lubricated state of rolls for the deformation. Under such state of deformation, the effectiveness of imposed asymmetry is strengthened in order to introduce more through thickness shear in a rolled sheet.

The strain rate was calculated for the rolling process by using the following equation from Ko et al. [51]:

$$(\dot{\varepsilon}) = \frac{\text{True strain at a given defomation } (\varepsilon)}{\mathrm{t_{avg}}} \tag{1}$$

$$t_{avg} = \frac{\text{contact length}}{\nu_{avg}} = \sqrt{\mathrm{R}\left(\mathrm{h_i} - \mathrm{h_f}\right) - \left(\frac{\mathrm{h_i} - \mathrm{h_f}}{2}\right)^2} \Bigg/ \left(\frac{2\pi n_{avg}}{60}\right)\mathrm{R} \tag{2}$$

Where, R is the roll mean radius, h_i and h_f denote the initial and final thickness of a sample and n_{avg} is the number of revolutions per minute (RPM). The strain in the deformation zone of symmetric rolling is:

$$(\varepsilon_{xx}) = ln\left(\frac{h_i}{h_f}\right) \tag{3}$$

In case of imposed asymmetric condition in rolling by means of different roll diameters, the strain path is considered to be non-uniform, i.e., the value of shear strain and equivalent strain varies through the thickness as compared to the rolling strain. However, shear can become uniform through the thickness [47,48] when thickness reduction per pass is high (≥50%) at roll diameters ratio like 1:1.6 and above. Under such scenario, the texture simulations rationalized the fact that the experimentally measured texture matches if only when deformation is decoupled, i.e., by first applying rolling strain in the entry zone of deformation and then shear strain effectively in the remaining deformation zone. The rolling strain remains effective in the entry part of the deformation zone and thereafter does not change in its value [48]. Thereby, in the present investigation, the measured value of shear strain in mid thickness of a rolled sheet was considered for the strain rate calculation.

If strain path is considered uniform in a given pass of rolling then the shear strain γ at a given point along the thickness can be calculated by [48,58]:

$$\gamma = \left(\frac{h_i}{h_i - h_f}\right) tan(\alpha_f) ln\left(\frac{h_i}{h_f}\right) \quad (4)$$

If it is considered that the effective mode of deformation is shear, then maximum shear strain γ_{max} that can be imposed is simply given by:

$$\gamma_{max} = tan(\alpha_f) \quad (5)$$

Here, α_f denotes the final angle of the inserted pin or the indentation marks on transverse direction plane with respect to the sheet normal after a given pass. It is about 70° when 75% thickness reduction is applied in one pass at room temperature with a roll diameters ratio of 1:2 [49]. The value of α_f decreases with smaller roll diameters ratio than 1:2. For the diameter ratios of 1:1.6 and 1:1.3, α_f angle values are 65 and 20°, respectively.

For the given configuration of symmetric rolls (100 mm roll mean radius, 34 r.p.m.) and specimen deformation geometry used in the present study, the applied 75% thickness reduction in one pass yields a strain of 1.38 ($\varepsilon_{eq} = 1.6$) and a strain rate in the order of ~30 s^{-1} at room temperature. Table 1 presents approximation of shear strain and strain rate for the roll diameter ratios 1:1.3, 1:1.6 and 1:2. It is noticed that the highest applied roll diameters ratio 1:2 can impose a strain rate about twice of what can be achieved by the symmetric rolling at room temperature by using eq. 1 from ref. [51]. Here in Table 1, it was assumed that the achieved thickness reduction in a pass at room temperature was same for all the roll diameters ratios. Nevertheless, the achieved final thickness was 1.75, 1.65 and 1.4 mm (65, 68 and 72% in thickness reduction) at the roll diameter ratios of 1:1 and 1:1.3, 1:1.6 and 1:2, respectively. However, with increase in warm rolling temperature, it is assumed that the effectiveness of imposed shear can increase the value of α_f angle and also the final achievable thickness after a given thickness reduction in a pass of rolling.

Prior to each warm rolling schedule, specimens were kept in furnace for 45 minutes to achieve required pre-selected deformation temperature uniformly. In addition to the ambient condition of rolling, four temperatures were selected between 250 °C to 700 °C for the warm deformation. The furnace was kept near the rolling mill so that the temperature drop in specimens can be minimized before they get their roll bite. The rolls of rolling mill were at room temperature. Similar as reported in the literature, a minimum temperature rise due to the adiabatic heating was observed in these experiments also [59].

For sample quenching, a cold-water filled container was stationed next to the rolls in such a way that the deformed specimens immediately fall in it, once they were released form the rolls. Precautions were taken in such a way that once the specimen released from rolls and its fall in water container should not exceed more than 3–4 seconds. This step enables to assist in freezing the deformed microstructure spontaneously [60]. Apart from instant quenching, some specimens were air cooled after deformation so that their microstructure can be compared with cold water-quenched specimens.

Table 1
Approximation of shear strain and strain rate for 75% thickness reduction in a pass with different set of roll diameters ratio at room temperature.

Roll diameters ratio	Pin inclination angle (α_f)	Shear strain		Strain rate (s^{-1})	
		Eq. (4)	Eq. (5)	Eq. (4)	Eq. (5)
1:1.3	20°	0.17	0.37	0.31×10^1	0.68×10^1
1:1.6	65°	0.98	2.14	1.81×10^1	2.14×10^1
1:2	70°	1.26	2.74	2.3×10^1	5.1×10^1

2.2. Orientation mappings and texture analysis

Microstructures and textures were investigated at the mid-thickness of a rolled sheet from Electron Back Scattered Diffraction (EBSD) scans along the ND-RD (2–1) plane, far from the front and tail ends. This section was chosen as it is the one in which plain strain condition of compression prevails during conventional (symmetric) rolling. It is also the most appropriate to judge the effectiveness of imposed asymmetry and the shear effect on the plain strain compression condition.

Prior to EBSD, samples were ground and mechanically polished using 9, 6, 3 and 1 μm diamond suspension followed by a final polishing with OP-S (Oxide Polishing Suspension) solution. A Zeiss LEO 1530 FEG-SEM equipped with a Nordlys II detector was used for EBSD mappings, with an accelerating voltage tension and probe current of 20 kV and 1 nA respectively.

The ATEX software [61] was then used for the complete data post-processing, analysis and display of images. All the conventional EBSD scanned maps were minimum of 160 μm × 220 μm in size for the high resolution and having step size in order of 0.1 to 0.2 μm. Although, the representative Inverse Pole Figure (IPF) maps in result section were truncated in similar size for the dynamic recrystallized grains statistics point of view. Apart from having smaller step size, all the samples were also scanned with 0.6 μm step size for the bulk texture measurement. The size of scanned and merged area for this purpose was in order of 3 mm in length and 0.5 mm in height The tolerance angle to define a grain was set 5° and grains with 3 pixels and below were excluded in grain size calculation. The microstructure is represented in IPF maps of the rolling direction (RD). For better visualization of microstructure in severely deformed condition, the grain boundaries of 15° and above were only delineated in all the conventional EBSD maps. The criteria based on grain internal disorientation average (also called grain orientation spread) was applied to distinguish recrystallized grains from the deformed ones [49]. Here, both terms of recrystallized and recrystallizing grain are used for the grains possessing a maximum internal disorientation average ≤ 2° which formed either by grain fragmentation or dynamic recrystallization. In Table 2, the largest common area fitting to all EBSD maps was considered to compare the average grain size, the recrystallized area fraction and grain ellipticity (which equals $1 - b/a$, a and b being the small and the big axis of the ellipse, respectively). The percentage of recrystallized fraction may slightly differ from the one written in the figures, as the latter is related to the displayed area.

The texture results are presented in $\phi_2 = 45°$ section of the orientation distribution function (ODF) where nearly all preferred texture components of shear and rolling can be seen. For both rolling and shear texture, the texture component identification and their ideal locations were taken from ref. [47]. Orientation within 10° from the ideal location were integrated to quantify the intensity in ODF and volume fraction of preferred texture components.

2.3. Grain internal disorientation and GND densities

In order to investigate the characteristics of dynamic recrystallized grains, grain internal disorientation angles and the geometrically necessary dislocation (GND) densities were measured by means of High-angular Resolution on-axis Transmission Kikuchi Diffraction (HR-TKD) [62,63]. HR-TKD is a very recent technique which couples the high-spatial resolution of the TKD technique (typically 6-12 nm laterally) with the high-angular resolution on lattice rotations provided by digital image correlation (DIC) techniques applied to high-resolution electron diffraction patterns (typically 0.01° for 1-megapixel patterns).

In “on-axis” TKD configuration, a thin foil is observed in transmission mode of the SEM, where the scintillator is placed beneath the specimen, perpendicularly to the electron beam [64]. The configuration offers 20 times faster acquisitions [65] and about 35% improved lateral spatial resolution [66] as compared to conventional “off-axis” TKD, which reuses the EBSD camera.

Table 2
Evolution of the area fraction of recrystallized and fragmented grains (partitioned part) and their average size and ellipticity as a function of temperature, roll diameter ratio and cooling conditions. The partitioning of the overall microstructure is based on internal disorientation average (≤ 2°) [49].

Temperature	Roll diameter ratio	Area fraction [%]		Average grain size [μm]		Average grain ellipticity	
		Water quenching	Air cooling	Water quenching	Air cooling	Water quenching	Air cooling
700 °C	1:1	1.90	52.56	1.8	19.07	0.42	0.40
	1:2	36.90	100	5.5	19.18	0.34	0.33
600 °C	1:1	1.0	1.0	1.1	1.17	0.46	0.45
	1:2	16.17	20.22	2.46	4.40	0.34	0.35
450 °C	1:1	–	1.9	–	0.84	–	0.47
	1:2	12.82	20.06	0.90	0.99	0.36	0.35
250 °C	1:1	–	5.4	–	0.81	–	0.49
	1:2	27.50	30.9	0.81	0.83	0.44	0.44
Room temperature	1:1	–	1.5	–	0.87	–	0.55
	1:2	–	18.52	–	0.95	–	0.47

The foils were prepared from twinjet polishing by using a mixture of 90% ethanol and 5% perchloric acid at 30 V at −20 °C. A Bruker e^{-}Flash^{HR+} camera attached to a Bruker OPTIMUS detector head for "on-axis" TKD was used in a Zeiss SUPRA 40 FEG-SEM. The latter was operated at 30 kV with a probe current 1.25 nA. Such an accelerating voltage makes the TKD technique selective in depth [67], which strongly reduces the occurrence of superimposed patterns as compared to transmission electron microscopy. TKD is therefore advantageous for the orientation mapping of nanostructures [68].

For all the displayed datasets, diffraction patterns of 600 × 600 pixels were recorded with a 16-bit grayscale. Each pattern results from the average of three patterns, each one captured with an exposure time of 24 ms (acquisition frequency of about 14 Hz). The pattern were post-processed in ATEX-software [61], in which the method proposed in [63,69] is implemented. Within each grain, a diffraction pattern was taken as a reference and compared to the ones forming the grain. From the measured displacement field between the two images, lattice rotations and elastic strains with respect to the reference point are deduced, knowing the SEM projection geometry (provided by Bruker ESPRIT 1.9 software).

Regarding the grain internal disorientation angle, two types of grain tolerance were considered: 5° and 0.3°. Note that grains smaller than 10 pixels were excluded in both cases. First, grains were detected in a standard way using the 5° criterion. It is the same as EBSD scans, but the grain boundaries are now plotted with tolerance angle of 5° and above (instead of 15° and above). The HR-TKD analysis was then carried out to obtain grain internal disorientation angles in the range of 0 to 12°. Regarding the second tolerance angle of 0.3°, it was chosen to highlight orientation gradients in the grain's substructures. However, such a tolerance angle is lower than the noise on the indexed crystallographic orientations (typically ≥0.5° for standard Hough-transform based indexing). Grains of very few pixels- or even single pixel are consequently detected everywhere, rather than sub grains themselves. Smoothing orientations is not a solution as sub grain boundaries (i.e., discontinuities) then vanish. To overcome this issue, TKD datasets were "re-indexed", knowing the orientation of the reference pattern within each grain and the relative lattice rotations measured by HR-TKD. It is detailed in appendix B. From the recomputed orientations, (sub) grains were successfully detected and the internal disorientation angles were deduced in the range 0 to 2°, without having to conduct another HR-TKD measurement. Similar to the maps with 5° grain tolerance angle, the grain boundaries in maps with 0.3° grain tolerance angle were also colored in black.

The tolerance angle of 5° was also opted for Geometric Necessary Dislocation (GND) densities. The norm of the Nye's dislocation tensor **α** is displayed in the range 1×10^{14} to 5×10^{16} m^{-2} using a logarithmic scale. Note that the bi-dimensional nature of TKD (but also EBSD) mappings prevents accessing the full tensor. Only the α_{i3} components are fully known while the contribution of elastic strain was neglected in α_{12} and α_{21} components. All the other terms were put to zero.

Finally, HR-TKD mappings were complement by fore-scattered electron diodes (FSD) images. Using three diodes positioned next to the scintillator (see [62]), the microstructure was finely visualized prior orientation mappings. Although, the FSD contrast depends on numerous factors (orientation, phase, thickness, topography…), here, it essentially displays orientation changes in a very sensitive way [62]. This is because a single phase is present (ferrite) while the sample thickness is relatively uniform over the observed region.

3. Results

3.1. Microstructure

Fig. 1 presents microstructure and bulk texture of initial material after heat treatment. The initial microstructure consists of globular shaped grains with average size of 36 μm. The intensity of texture is very weak as represented by the $\phi_2 = 45°$ section of the Orientation Distribution Function (ODF). Such initial conditions of specimen are comparable with earlier investigation carried out on extra-low carbon steels by warm symmetric rolling [40].

Figs. 2a and 3a present overall IPF maps in the rolling direction at mid thickness for warm rolled and water quenched sheets at 700 °C and

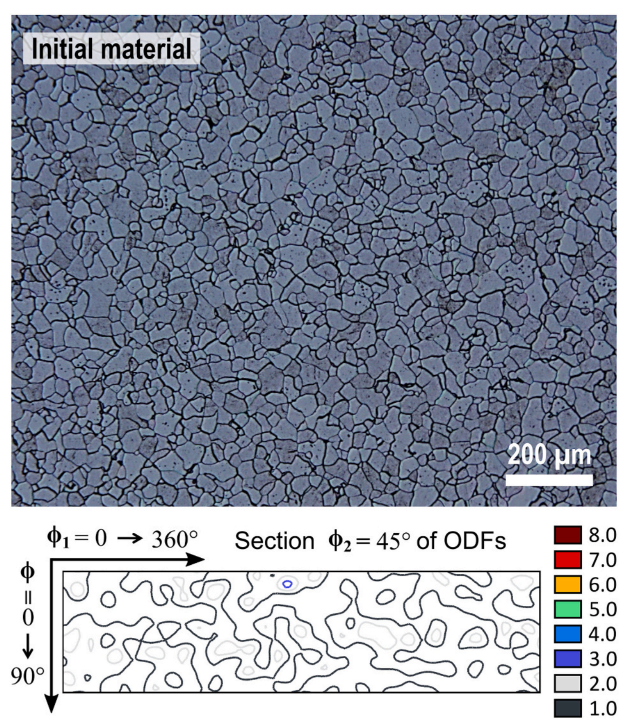

Fig. 1. Initial microstructure and texture after heat treatment at 1050 °C.

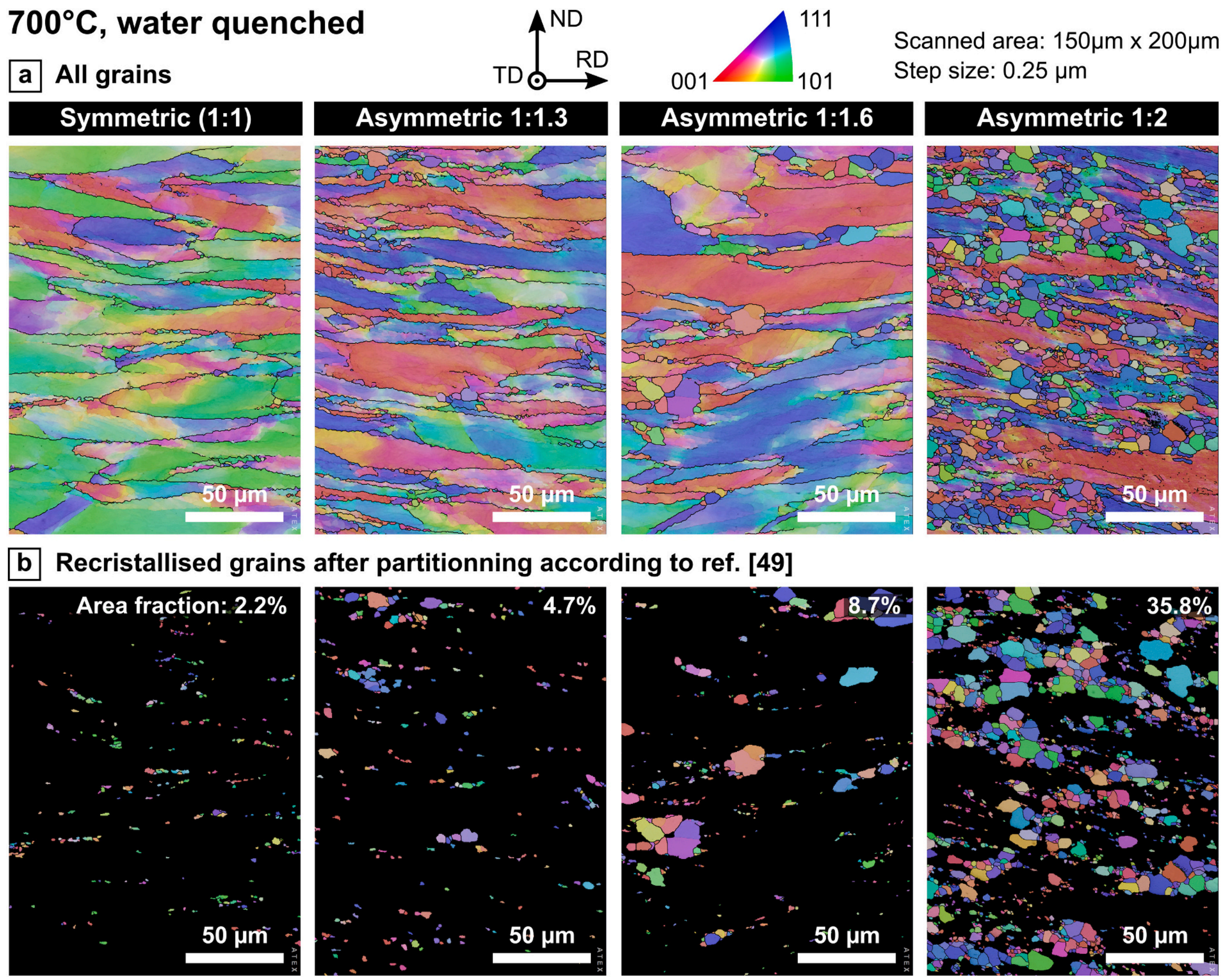

Fig. 2. IPF maps of the rolling direction (RD) (a) without and (b) with grain partitioning for 700 °C warm rolling by the roll diameters ratio between 1:1 to 1:2 and water quenched.

600 °C. With increase in roll diameters ratio, a noticeable orientation change occurs in the elongated bands of original grains in the microstructure. At roll diameters ratio 1:2, the recrystallized grains are quite noticeable as compared to other cases of rolling. In order to have closer inspection of recrystallized grains, Figs. 2b and 3b present them separately from the overall microstructure by using filter which is based on the criteria of grain internal disorientation average and the grain size [49]. The grain partitioning clearly presents increase in area fraction of recrystallized grains and in their sizes as the roll diameters ratio increases from 1:1 to 1:2 (Table 2). Nevertheless, with decrease in temperature from 700 °C to 600 °C, average grain size and fraction of recrystallized grains reduced at both symmetric and asymmetric cases of rolling (Table 2).

The case of air-cooling on deformed microstructure at 700 °C and 600 °C is shown in Fig. 4 where IPF maps are presented only for the symmetric (1:1) and asymmetric ratio of 1:2 where significant changes in the microstructure are visible. At roll diameters ratio 1:2, a fully recrystallized microstructure formed at 700 °C (left side) and partial recrystallization occurred at 600 °C (right side). The recrystallized grains formed at 600 °C are a mixture of small and some slightly larger equiaxed grains. They evolved preferentially along the boundaries of original grains but now a very few of them also formed along the deformation bands that reside in the elongated bands. For symmetric rolling, specimen shows uncomplete recrystallization at 700 °C. Whereas, a few very fine recrystallized grains formed sparsely when temperature reduced to 600 °C. The comparison of symmetric and asymmetric (1:2) cases of rolling with air colling presents significant difference in the recrystallization kinetics with decrease in deformation temperature just from 700 °C to 600 °C (Table 2).

After observing recrystallization at 700 °C and 600 °C, warm rolling was carried out at lower temperatures. At this stage, only roll diameters ratio 1:1 (symmetric) and 1:2 (asymmetric) were continued to use. Fig. 5 presents IPF maps of water quenched and asymmetric (1:2) rolled at 450 °C and 250 °C. It was noticed that recrystallized grains formed along the elongated bands of original grains at 450 °C. Although, formation of few dynamically recrystallized grains was also noticed at the deformation bands that lie inside the elongated original grains. At 450 °C, the average grain size is further reduced as compared to the upper warm temperature range (600–700 °C) of rolling (Table 2). Here, recrystallized grains form a necklace type of structure around the grain boundaries of original grains.

At 250 °C, the microstructure appears quite severely deformed, and it is significantly different than the observed microstructure at 450 °C and above. The original grain bands are more fragmented and deformed severely at 250 °C to form fine grains than at 450 °C, where they are softened and seemed to be more in recovery process. It also appears that the grains recrystallized at 250 °C are more frequently to show partially separated grain sites (in magnified view). Still considering a roll diameters ratio of 1:2, air-cooled samples at 450 °C and 250 °C in Fig. 6a show quite similar microstructures compared to the water quenched ones (Fig. 5). They are having globular shaped fine recrystallized grains but more recovered original grain bands than the water quenched samples. The microstructure of symmetric (1:1) rolled and air-cooled samples in Fig. 6b are completely different from what was observed in

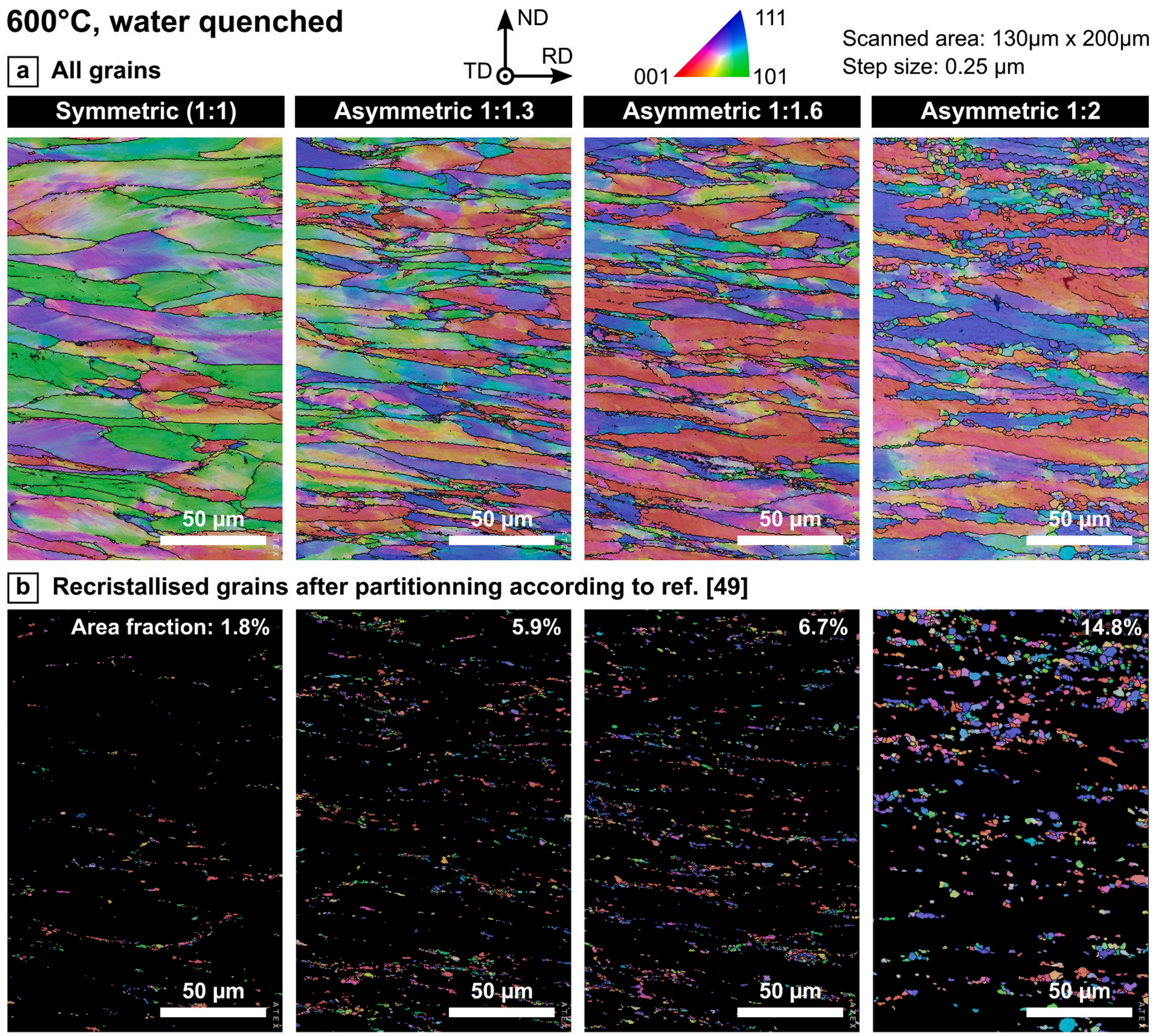

Fig. 3. IPF maps of the rolling direction (RD) (a) without and (b) with grain partitioning for 600 °C warm rolling by the roll diameters ratio between 1:1 to 1:2 and water quenched.

asymmetric case at 450 °C and 250 °C. The deformed microstructure mainly consists of thick bands of original grains and shear bands. At 250 °C (right side), the frequency of shear bands is higher than that at 450 °C (left side), which also means that more softening and recovery took place at 450 °C than 250 °C in symmetric rolled samples.

In order to compare the warm rolled samples with the room temperature deformed microstructures, the latter are presented in Fig. 7 (left side). The room temperature deformed microstructure of symmetric rolled sample appears to be similar to what was observed at 250 °C but with fewer frequency of shear bands. Nevertheless, the asymmetric rolled sample (Fig. 7a) is more severely deformed than the symmetric case (Fig. 7b). The partitioning of grains (right side), based on the same criteria as used earlier, presents the fragmented and fine grains throughout the microstructure which also mean their formation favored by the grain fragmentation process.

3.2. Texture

The overall textures, which include both deformed and recrystallized grains, and the texture formed by exclusively of recrystallized grains at 700 °C and 600 °C are presented in Fig. 8. It is noticed that the overall texture which forms during symmetric rolling shifts towards shear texture with increase in asymmetric ratio from 1:1.3 to 1:2. Nevertheless, the texture of recrystallized grains at 700 °C has less impression of shear texture than at 600 °C where it evolves effectively as the roll diameters ratio increases up to the 1:2. Fig. 9 presents the overall texture and the texture formed in the recrystallized and fragmented grains at 450 °C to room temperature at the roll diameters ratio of 1:2. The overall texture and the texture of partitioned grains below 450 °C are quite similar to each other. It means that shear texture prevails both in recrystallized and fragmented grains when sample warm rolled below 450 °C at roll diameters ratio 1:2. Although, shear texture formed by the partitioned grains is weaker than that of the overall map.

The texture measured from the EBSD scanned maps of about 3 mm in length and 0.5 mm in height were compared with the bulk texture measured from the X-ray diffraction on 30 mm × 30 mm sized ND surface at the mid thickness of the samples. The measured bulk texture results between room temperature and 600 °C by EBSD and X-ray diffraction for the asymmetric rolling are separately put in appendix A to maintain the consistency of the paper.

From Figs. 8 and 9, it is clear that the overall texture intensity has increasing trend with increase in temperature and presents a possibility of its decrease in value after 600 °C onwards.

The comparison between shear and rolling components can be

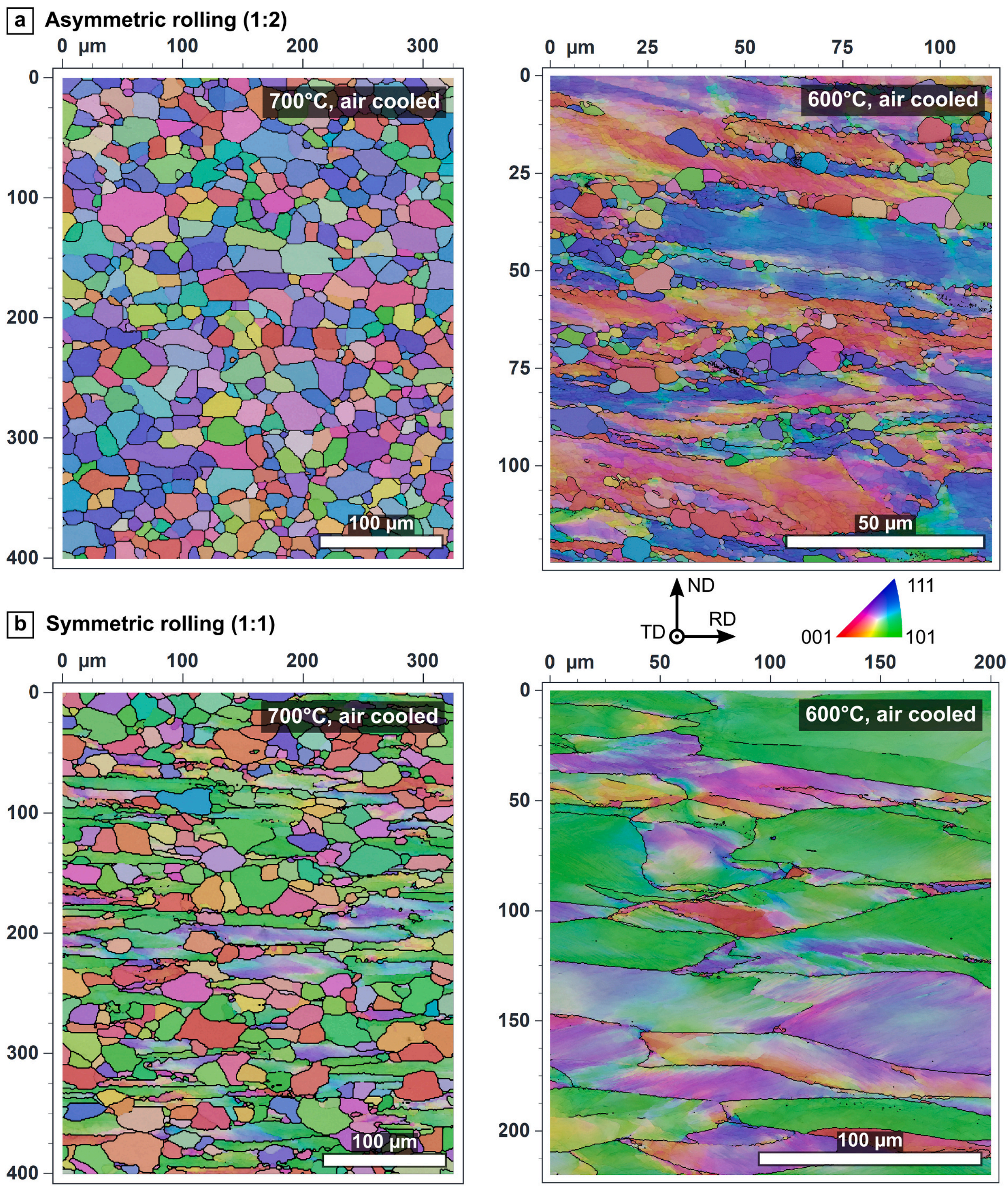

Fig. 4. IPF maps of the rolling direction (RD) of (a) asymmetric (1:2) and (b) symmetric (1:1) rolled samples at 700 °C (left) and 600 °C (right) and cooled by air.

delicate. Indeed, the shear components are metastable, grains can leave a component when the amount of shear increases. On contrary, the rolling texture components are stable and continuously rise as the sheet is rolled. As a consequence, Fig. 10 displays the intensity of the main peaks of the ODF located near the ideal components as well as the chosen texture of partitioned grains.

Overall, both ODF intensity (left) and volume fraction (right) up to 600 °C remain stronger in shear texture components than the rolling texture components in these asymmetric rolled samples. Interestingly, it is noticed that volume fraction of shear texture components is in decreasing order at 250 °C as compared to the room temperature. It mean that the negative strain rate sensitivity and the flow stress at 250 °C, which favors increase in fragmentation of grains also oriented dynamically recrystallized grains towards the rolling texture [27,40]. At 450 °C, original grains become softer with increase in temperature and absence of negative stain rate sensitivity led to the less number and area fraction of dynamically recrystallized grains than what observed at 250 °C.

At 700 °C, the strength of ODF intensity and volume fraction of shear texture components decreases as compared to the 600 °C and below. It is mostly due to the increased thermomechanical activities and the growth of dynamically recrystallized grains which also favors other orientations

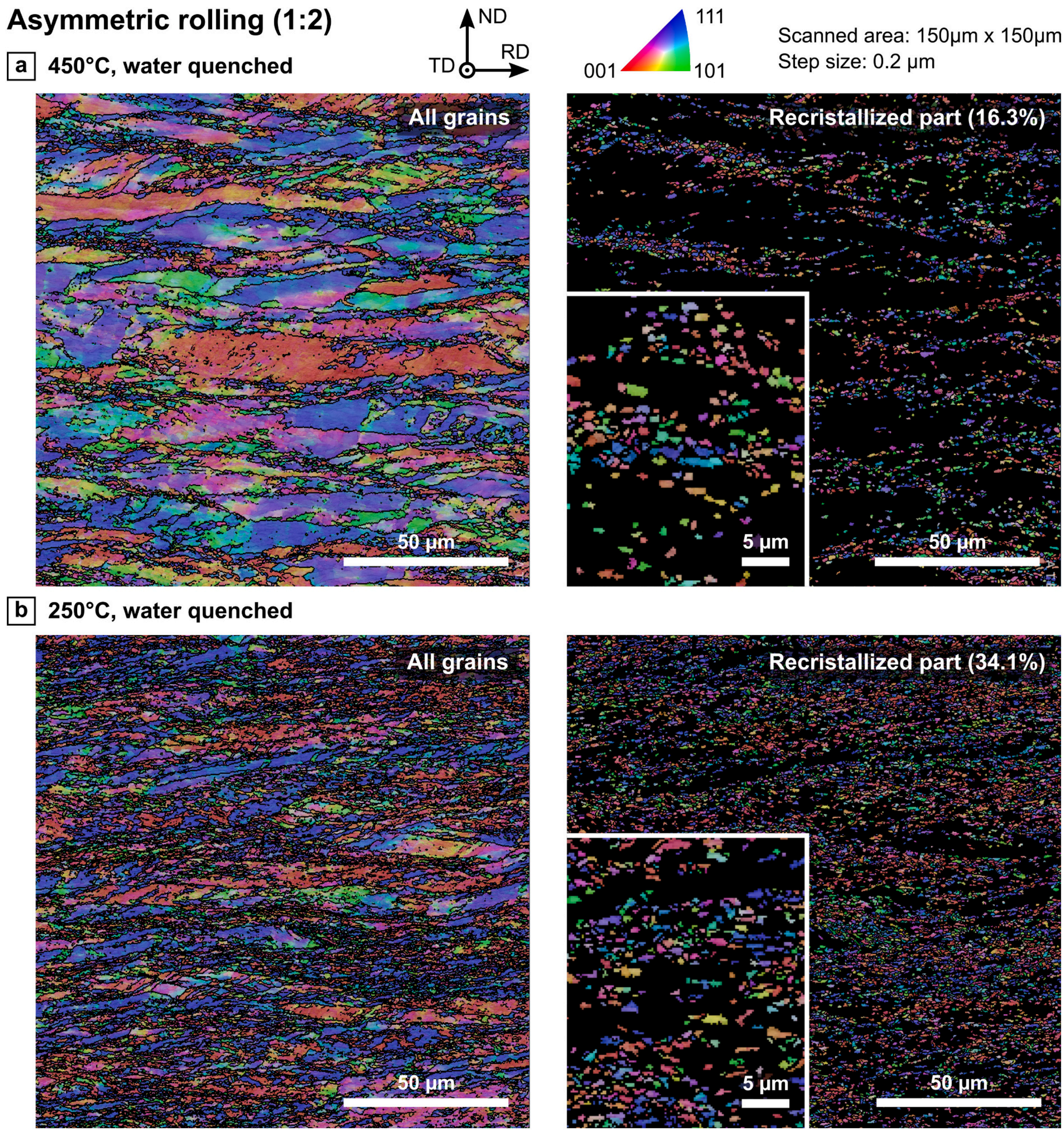

Fig. 5. IPF maps of the rolling direction (RD) without (left) and with (right) grain partitioning for asymmetric (1:2) rolled samples at (a) 450 °C and (b) 250 °C and water quenched.

to form along with those were rationalized by the type of deformation applied. Moreover, a regained strength in symmetric rolling texture components is noticeable. A regained strength in symmetric rolling texture components of dynamic recrystallized grains could also suggest that after nucleation, their growth might be affected by the softened and thinner original elongated bands at 700 °C (Fig. 2). The thinner elongated bands can constrain the growth of dynamically recrystallized grains by their own boundaries as well as the impingement of growing grains with each other in these elongated thinner bands. Therefore, the dynamically nucleated grains by shear were possibly unable to reach at their preferred locations in Euler space and end up favoring the rolling texture components or a random orientation. It is also possible that increased kinetics of dynamic recrystallization at 700 °C promotes having more nucleation sites where grains with rolling texture might also have formed independently and grown to increase in its volume fraction.

It is important to note that the new fragmented or dynamically recrystallized grains form in a condition where ease in shearing occurs as the deformation temperature increases, thus ease in grain rotation also. In absence of shear, dynamic recovery prevails rather than increase in area fraction of recrystallized grains in rolling (Figs. 4b, 6b, 7b). In fact, shear texture components in asymmetric rolling are directly related to the preferred rolling texture components by 30–35° rotation about the TD direction [47]. Therefore, with increasing deformation temperature and ease in shear, a shear texture is more likely than a rolling one.

The Zener-Holloman Parameter ($Z = \dot{\varepsilon}\, exp\left(Q/_{RT}\right)$) is considered to define whether a deformed microstructure would dynamically recover or recrystallize. Here R is the gas constant (8.317 J/mol K), T is absolute deformation temperature and Q is the activation energy. In literature, different values of activation energy were used on the basis of material

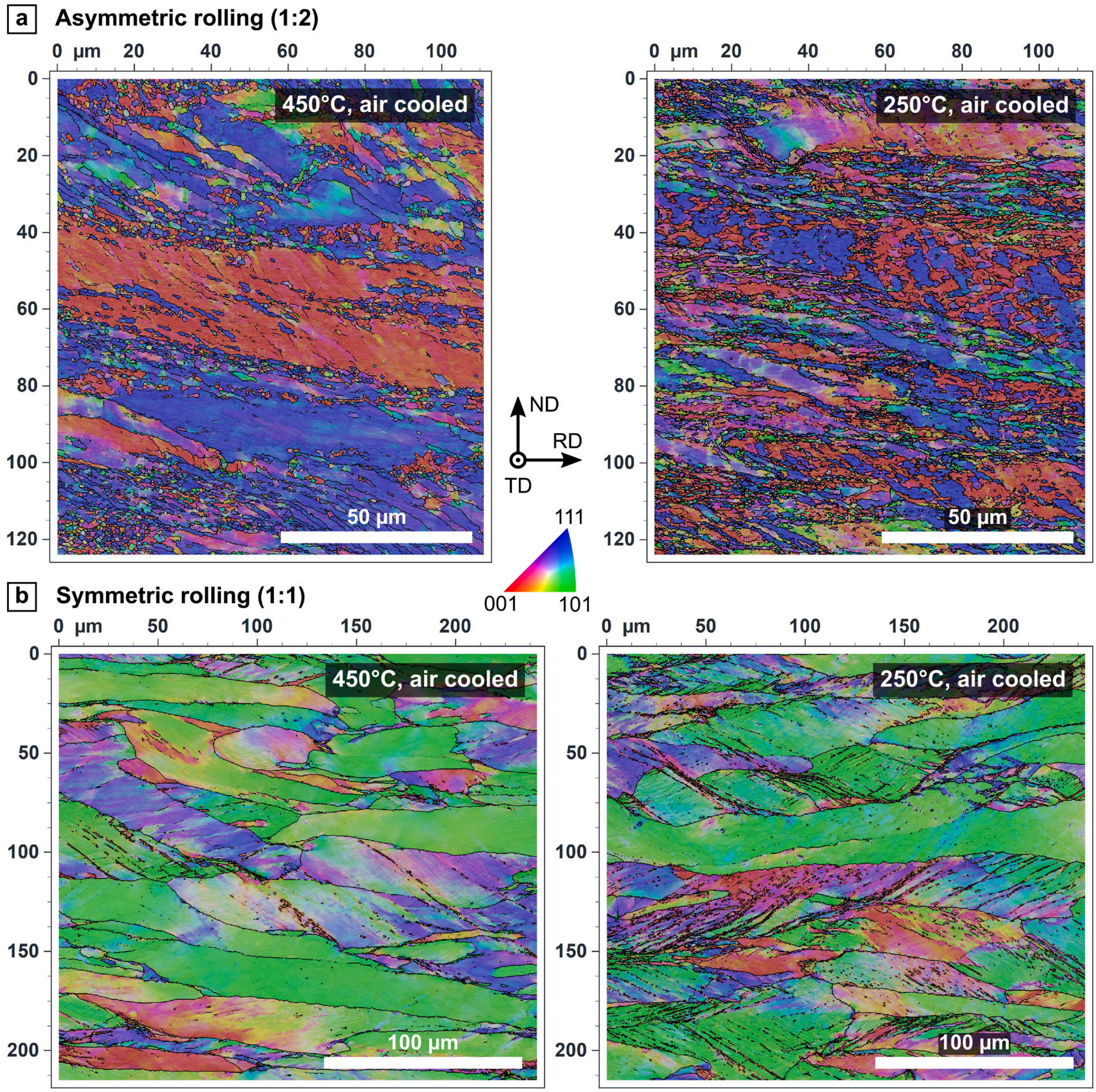

Fig. 6. IPF maps of the rolling direction (RD) of (a) asymmetric (1:2) and (b) symmetric (1:1) rolled samples at 450 °C (left) and 250 °C (right) and cooled by air.

composition and the deformation conditions. Therefore, the activation energy of self-diffusion in ferromagnetic ferrite iron about 254 kJ/mol was taken into account for the estimation of Z parameter [59]. A high Zener-Holloman parameter (lower temperature and high strain rate) result in dynamic recovery while its low value (higher temperature and lower strain rate) defines the state of dynamic recrystallization in the microstructure. The Zener-Hollomon parameter is calculated for both symmetric case and for the maximum roll diameters ratio (1:2) in asymmetric case. The calculated values of Zener-Hollomon parameters from room temperature to 700 °C are presented in Table 3.

3.3. HR-TKD

The results from HR-TKD analyses (as detailed in section 2.3) are presented in Figs. 11 to 14 for four temperatures: 700 °C, 450 °C, 250 °C and ambient. These figures are subdivided into four types of images: (a) a forescatter electron diode (FSD) image; (b) the internal disorientation angle of grains defined with a grain tolerance angle of 5° and (c) the corresponding GND densities; (d) the internal disorientation in grain substructures (grain tolerance of 0.3°).

It is noticed that forescatter images (Figs. 11–14a) show change in both grain size morphology as well as inherent features with temperature. Their realization and quantification in terms of GND density (Figs. 11–14d) clearly agrees with FSD observation. A higher GND density is present within internal core of a grain as well as next to the substructure dislocation walls as the temperature decreases. It is also observable that grains which appeared gray-colored in 0° to 12° internal disorientation (Figs. 11–14b), has disorientation profile from 0° to 2° if the grain tolerance angle selected is 0.3° instead of 5° (Figs. 11–14d, see methodology part).

4. Discussion

It was noticed from the IPF maps in Figs. 2–7 that both deformation and equiaxed grain formation kinetics were profoundly affected by the change in rolling parameters and temperature. Therefore, analysis is sub-sectioned in two parts: (i) Occurrence of dynamic recrystallization and (ii) Characteristic of dynamic recrystallized grains.

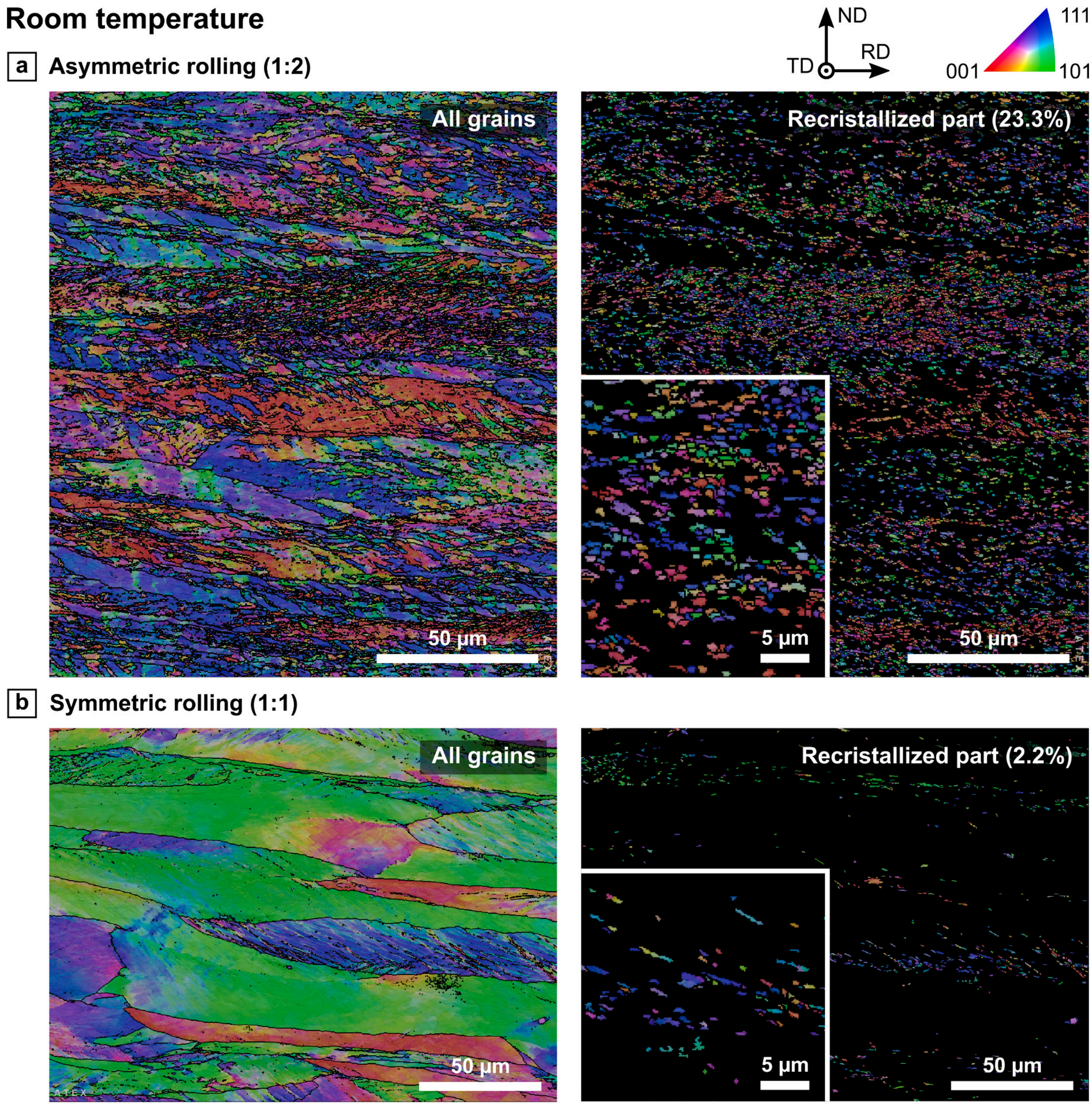

Fig. 7. IPF maps of the rolling direction (RD) without (left) and with (right) grain partitioning for (a) asymmetric (1:2) and (b) symmetric (1:1) rolled samples at room temperature.

4.1. Occurrence of dynamic recrystallization

The possible reason of having absence of dynamic recrystallization and prevailed dynamic recovery in symmetric rolling can be anticipated from the Zener-Holloman Parameter. From Table 3, except the upper warm temperature (700 °C), Z parameter values associated with lower temperatures are too high [59,70–74]. Although, the onset of dynamic recovery/restoration in ferritic steels is influenced by alloying elements and the testing conditions. It might be therefore difficult to compare results precisely about the onset of dynamic recovery/restoration. However, it can be noticed that the most of investigations for low-carbon steels roughly agree on the Z parameter value about 10^{15} or below for the onset value of dynamic recrystallization [70–74]. The present study also reveals the prevalence of dynamic recovery rather than the dynamic recrystallization above this value of Z parameter in warm deformation of low-carbon steels.

Examination of other investigations on plane strain compression or torsion tests with similar average grain size of 40 μm or with large grains, it was noticed that dynamic recrystallization mostly occurs in the upper range of ferrite warm temperature (700 °C and above) [27,33,70–74]. It was also reported that for a given strain rate, a higher thickness reduction per pass is more favorable for the initiation of dynamic recrystallization than the small thickness reduction per pass [7,75].

The occurrence of only few very fine equiaxed grains along the grain boundaries and their junctions in water quenched samples of symmetric rolled at 700 °C and 600 °C (first column in Figs. 2 and 3) is apparently due to the onset of discontinuous dynamic recrystallization. Although, these equiaxed grains are very fine but some of them are well defined and surrounded by high angle boundaries ≥15°. Having very few fine equiaxed grains along with elongated bands were also observed in deformed and water quenched microstructures of Ti—Nb stabilized IF (interstitial free) steel in the temperature range of 750 °C–850 °C [25,26,32]. The presence of fine equiaxed grains was explained by the occurrence of dynamic recrystallization along with dynamic recovery. Therefore, it is anticipated that observed few very fine equiaxed grains

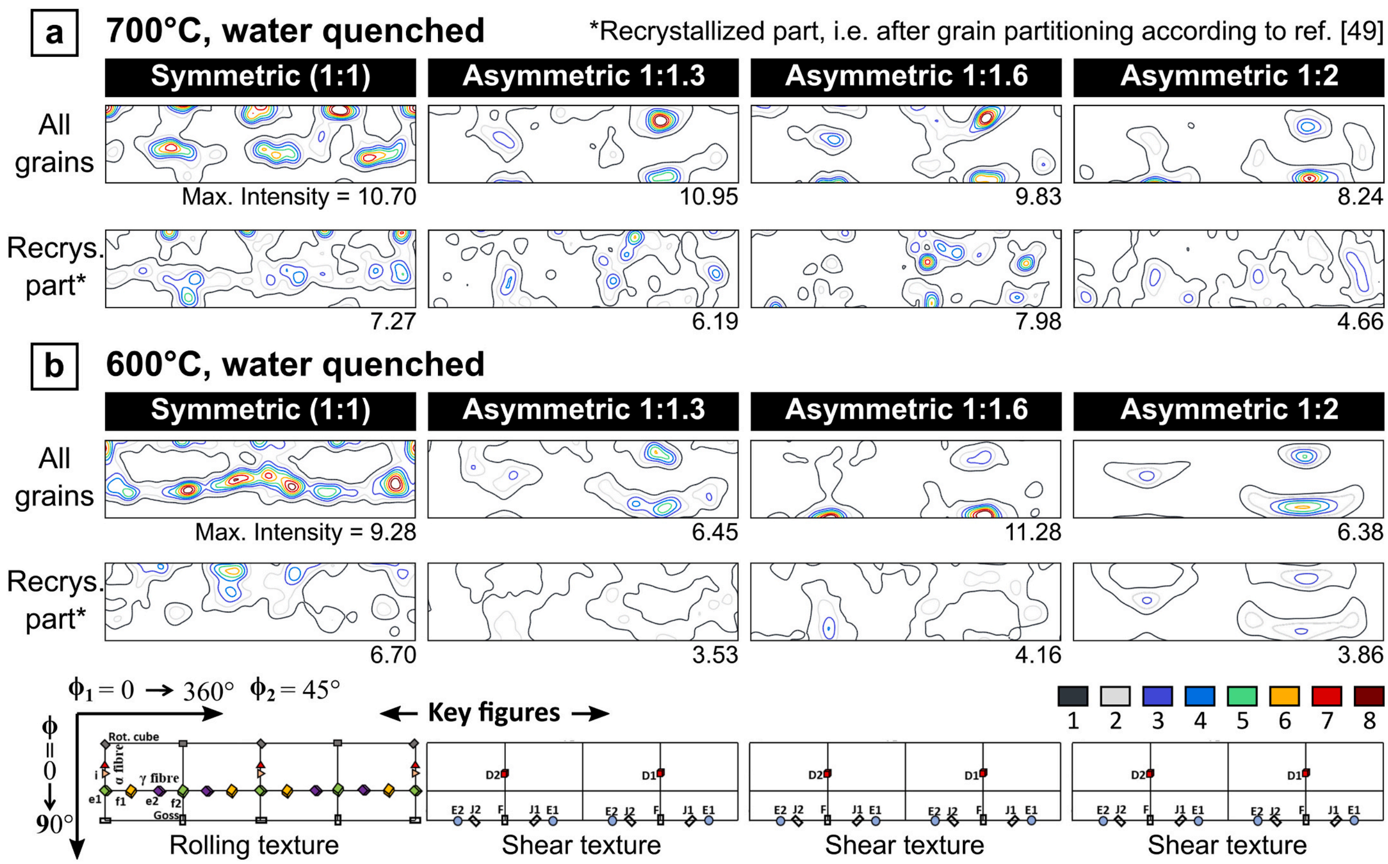

Fig. 8. $\phi_2 = 45°$ ODF sections of samples rolled with roll diameters ratio 1:1.3, 1:1.6 and 1:2 at temperatures of (a) 700 °C and (b) 600 °C and water quenched, followed by key figures showing the ideal location of texture components.

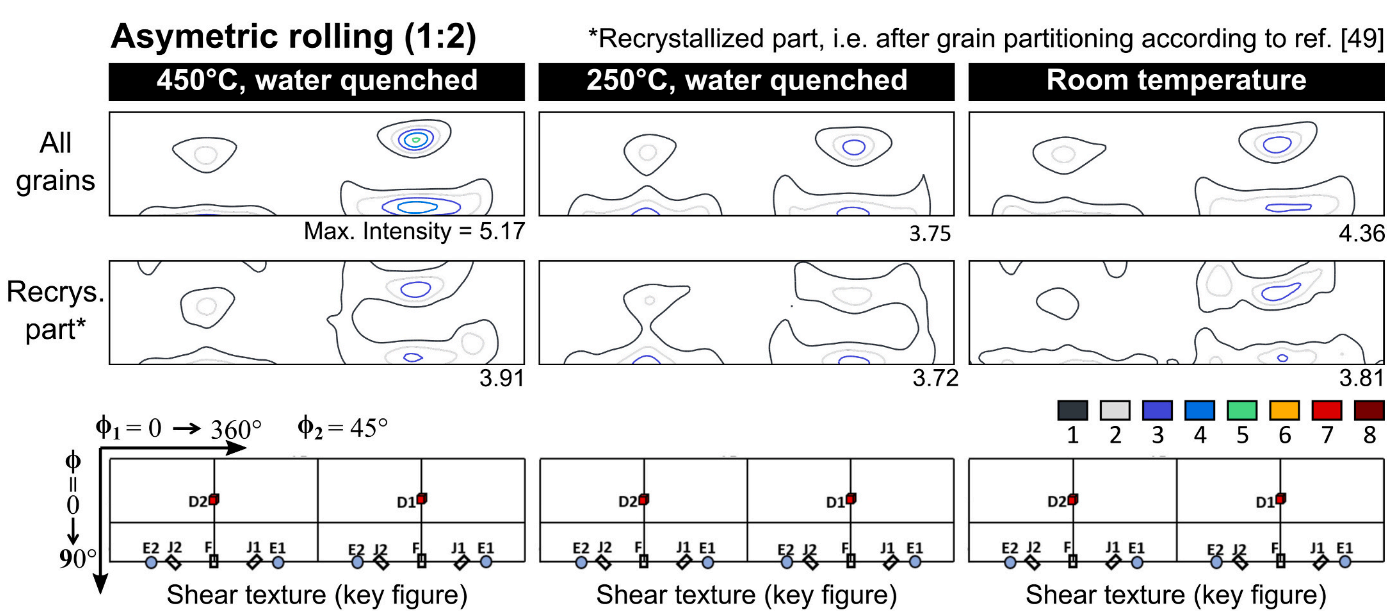

Fig. 9. $\phi_2 = 45°$ ODF sections of samples rolled with roll diameters ratio 1:2 at 450 °C, 250 °C and room temperature and water quenched followed by key figures showing the ideal location of shear texture components.

at 700 °C and 600 °C in water quenched microstructures are actually representative of the onset of discontinuous dynamic recrystallization in assistance to the dynamic recovery. Since the dynamic recovered elongated bands prevails in water quenched samples at both 600 °C and 700 °C, it is possible that observed very fine and sparsely distributed grains of discontinuous dynamic recrystallization cannot be observed easily if sufficiently large map is not acquired by EBSD.

In case of asymmetric rolling with roll diameters ratio 1:1.3 to 1:2 (second to fourth column in Figs. 2 and 3), dynamically recrystallized grains occurred in distinguishable sizes and fractions as compared to the

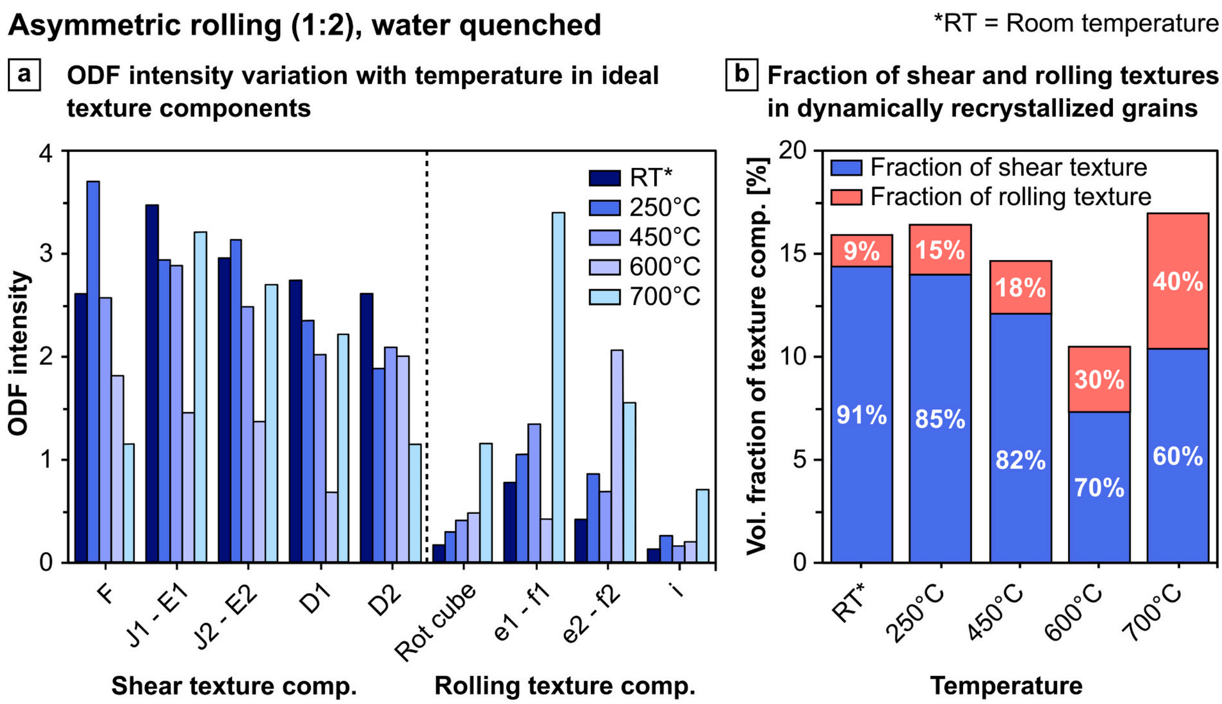

Fig. 10. Change in (a) ODF intensity of shear and rolling texture components and (b) volume fraction of shear and rolling textures in partitioned grains at roll diameters ratio 1:2 with increase in temperature from ambient condition to 700 °C.

Table 3
Zener-Hollomon Parameter for symmetric and asymmetric roll diameters ratio 1:2.

Temperature	Zener-Hollomon parameter [s^{-1}]		
	Symmetric (1:1)	Asymmetric (1:2) by Eq. (4)	Asymmetric (1:2) by Eq. (5)
700 °C	1.11×10^{15}	1.0×10^{15}	2.18×10^{15}
600 °C	4.05×10^{16}	3.6×10^{16}	7.9×10^{16}
450 °C	5.76×10^{19}	5.2×10^{19}	1.13×10^{20}
250 °C	6.01×10^{26}	6.8×10^{27}	1.16×10^{27}
Room temperature (27 °C)	$4.32 \times 10^{+45}$	3.8×10^{45}	8.27×10^{45}

dynamically recovered grains by symmetric rolling at both 700 °C and 600 °C. The possibility of such observation is due to simultaneous action of two things. First is the reduction in spring back effect of rolling mill by imposing asymmetric condition. Second is the contribution from texture rotation and effective plastic strain owing to the imposed shear. It could be the main reason for increase in both distinguishable size and fraction of dynamic recrystallized grains.

It is reported that in asymmetric rolling, a little higher thickness reduction achieved due to the reduction in spring back effect of rolling mill as compared to the symmetric case for the same rolling parameters, thus, thickness reduction in rolled sheet is more effective [76]. In accord to ref. [76], the effective thickness reduction increased as the roll diameters ratios changed from 1:1 to 1:2. Nevertheless, expected increase in strain rate value is not so high, despite considering roll diameters ratio 1:2 as compared to the symmetric case (~30 s^{-1}). Then, the whole range of calculated values of Zener-Hollomon parameter (function of strain rate and temperature) in Table 3 are similar for the symmetric and asymmetric rolling mills, thus, it supposed to still present dynamic recovery and a few very fine equiaxed grains. In reality, that is not the case.

Another additional aspect that could contribute in having increased dynamic recrystallization activities is the adiabatic heating. Although, increase in temperature just by imposing asymmetry might not be very significant as compared to the symmetric case. It is reported that the adiabatic heating can increase temperature about 12 °C to 40 °C for a corresponding decrease in applied temperature from 650° to 500 °C in similar deformation condition as used in the symmetric case [59]. Thereby, a prominent change in the microstructure due to just by adiabatic heating can be ruled out for the asymmetric case of rolling as well.

Apart from increased effectiveness in thickness reduction, the most convincing reason is to consider, the role of texture rotation for the observed change in microstructures. In Figs. 2 and 3, a small change in deformation mode by increasing roll diameters ratio from 1:1 to 1:1.3 has noticeably changed the grain orientations in microstructure and also assisted in increased fraction of fine grain formation of dynamic recrystallization. With increase in roll diameters ratio from 1:1 to 1:2, the rolling texture rotates to the regime of ideal shear texture and its effect reflected in terms of increased fraction of equiaxed dynamically recrystallized grains (Fig. 8). There are experimental evidences which show that, for a given value of strain, higher density of geometrically necessary dislocations (GND) is achieved in simple shear (torsion test) than in tension (traction test) [77]. Similarly, it has been also reported that torsion test can yield to a greater number of higher angle boundaries than in a rolled (plane strain compression) material as the grain shape is not constrained to remain flat in case of torsion test [78]. In fact, a comparison between symmetric rolling and shear based equal channel angular extrusion (ECAE) showed a higher grain refinement in ECAE due to increase in lattice rotation rate [79]. Thereby, if a deformation process favors texture rotation towards shear type texture, then its microstructure is prone to have arisen in instabilities by increasing GND density, leading to the increase of the fraction of high angle grain boundaries and of the fragmentation of grains.

The elongated boundaries of original grains also have tendency to form serrations or zig-zag feature on it. Mostly due to the origination and termination of types of bands such as shear, micro, deformation etc. and impurities at the grain boundaries. These are the possible sites where instability arises and eventually affects the GND density at the grain boundaries and area in their vicinity. With increase in effectiveness of

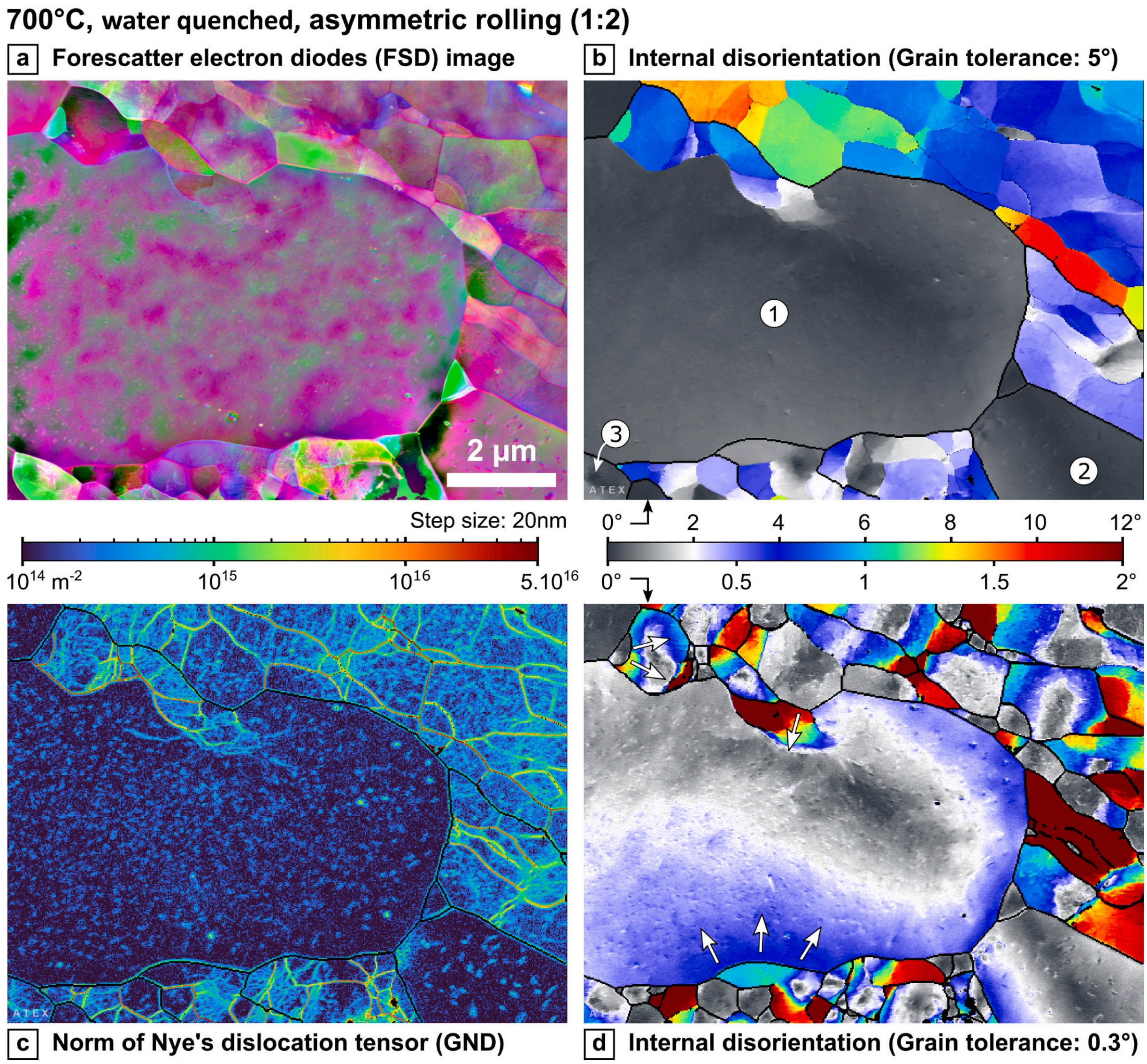

Fig. 11. HR-TKD analysis of sample rolled with roll diameters ratio 1:2 at 700 °C temperature and water quenched. (a) FSD image. (b) Internal disorientation angle of grains defined with a tolerance angle of 5°. (c) GND densities associated to (b). (d) Internal disorientation angle of grains defined with a tolerance angle of 0.3° after re-indexing.

imposed shear, thus the rotation of rolling texture, the serrations or zig-zag marks on grain boundaries undergo localized boundary rotation to overcome arisen instability. At room temperature, new grains also form at these sites but at warm or high temperatures deformation, the sites are for the discontinuous dynamic recrystallized grain formation. In present investigation, with increase in temperature, original grains become soften and the imposed shear tries to shear them and to rotate the localized area at or next to the serrations or zig-zag mark formation sites on the grain boundaries. Such localized rotation accompanied with grain boundary shearing and/or sliding leads to the change in local orientation and strain gradient that can lead to the formation of new grains at the grain boundaries [80–85]. Thereby, its effect on the discontinuous dynamic recrystallized grain formation which can also lead to the necklace structure formation at the grain boundaries.

It can now be conclusively said that the rotation of rolling texture to shear texture is the main contributor along with the effectiveness of thickness reduction and small increment in strain rate, leads to the observed dynamic recrystallization with imposed asymmetry. Without interference of shear on plane strain condition, the microstructure would present dynamic recovery for the same rolling parameters as used with imposed asymmetry.

4.2. Characteristics of dynamically recrystallized grains

The change in microstructure with increase in roll diameters ratio was prominent at the ratio 1:2. Thereby, this ratio was considered to be suitable to better examine dynamically recrystallized grains and their type in the temperature range of 700 °C to room temperature (water quenched).

Generally, a microstructural map which is acquired by the standard EBSD detector can be partitioned on the basis of grain internal disorientation filter of ≤2° for the recrystallization in deformed matrix [49]. Having high angle disorientation between adjacent grains is an additional parameter to define them as recrystallized grains. However, this method is insufficient to examine dynamically recrystallized grains specifically when concern is about substructures within a grain. Additional information such as trapped substructures, dislocations or precise disorientation profile within grains are required [26]. Thus, high-angular resolution on-axis TKD (HR-TKD) measurements were conducted to extract this relevant information. The results are presented in

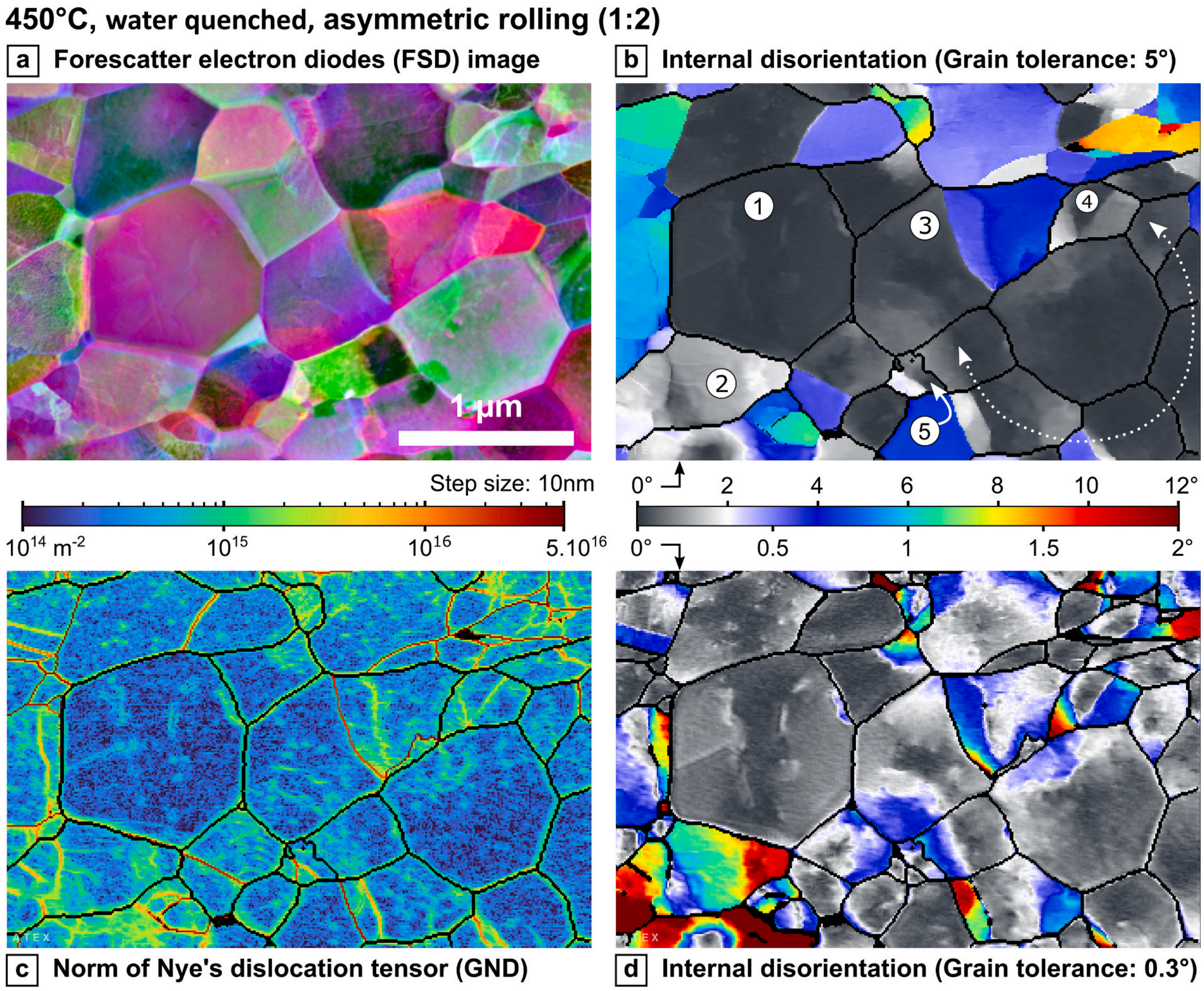

Fig. 12. HR-TKD analysis of sample rolled with roll diameters ratio 1:2 at 450 °C temperature and water quenched. (a) FSD image. (b) Internal disorientation angle of grains defined with a tolerance angle of 5°. (c) GND densities associated to (b). (d) Internal disorientation angle of grains defined with a tolerance angle of 0.3° after re-indexing.

Figs. 11 to 14, each one being associated to a given temperature. As mentioned earlier in section 2.3, two types of tolerance angle were used in Figs. 11 to 14. The 5° grain tolerance angle was used to detect and delineate the grains having their constituting boundaries of 5° and above. The 0.3° grain tolerance angle was used to find internal disorientation in the dynamically recrystallized grains and also within the substructures of a grain defined earlier with 5° tolerance angle. After defining substructure as a grain with 0.3° tolerance angle (map (d) of Figs. 11 to 14), the grain boundaries of 0.3° and above were traced in same color as used for the maps (b) of Figs. 11 to 14 for the 5° and above.

At 700 °C, some of dynamically recrystallized grains are large as compared to other grains (partitioned part in Fig. 2). These formed large grains raise the question whether or not static annealing took place to make them strain free within the interval of 3 to 4 seconds between roll exit and water quenching. Given the maximum disorientation of 2° for grain partitioning [49], these grains are spotted by numbers in Fig. 11b (700 °C), which shows the grain internal disorientation angle measured by HR-TKD. High-angular resolution mappings clearly present that these grains possess disorientation profile within 2° from internal core to their grain boundaries (Fig. 11d) and contains GND at the substructures (Fig. 11c, especially in grain #3 and at the top of grain #1). Thereby, these pretending to be large grains also fulfil all essential requirements to be termed as dynamically recrystallized grains as shown in maps of the Fig. 11 [26].

Overall, irrespective of grain sizes, these dynamically recrystallized grains show increase in disorientation in local areas next to adjacent grains, as highlighted by arrow in Fig. 11d. With increased effectiveness of plastic strain owing to the imposed shear, the elongated grains become thinner than the grains in symmetric rolled microstructure (Fig. 2). The growth front of dynamically recrystallized grains, which nucleate at grain boundaries, migrates into the inside of the elongated bands of the original grains. The growth front will have some disorientation distribution as compared to its central region which mostly remains in a strain-free state. It is possible that the growth front of large dynamically recrystallized grain as showen in Fig. 11d is impinged by another dynamically recrystallized grain which could be of any size. Impingement in the proximity of a smaller grain is probably due to being formed later than the larger grain as it had already been originated by the advantage of growing from the grain boundaries. Being confined to smaller size could also be due to the constraints of surrounding grains on it. It is also possible that within a short time, a few cycles of dynamic recrystallization occur, leading to the impingement between dynamically grown grains in different cycles. Such circumstances can also lead to the strain hardening of a dynamically recrystallized grain after the impingement by the growing grains, thus a change in disorientation distribution near or at the confronting area of the grain boundary [84].

It confirms that the nature of dynamic recrystallized grains at 700 °C is discontinuous type and its onset occurred during the deformation. Also, the interval of 3 to 4 seconds in water quenching is perhaps essential to observe dynamic recrystallization in a single pass rolling.

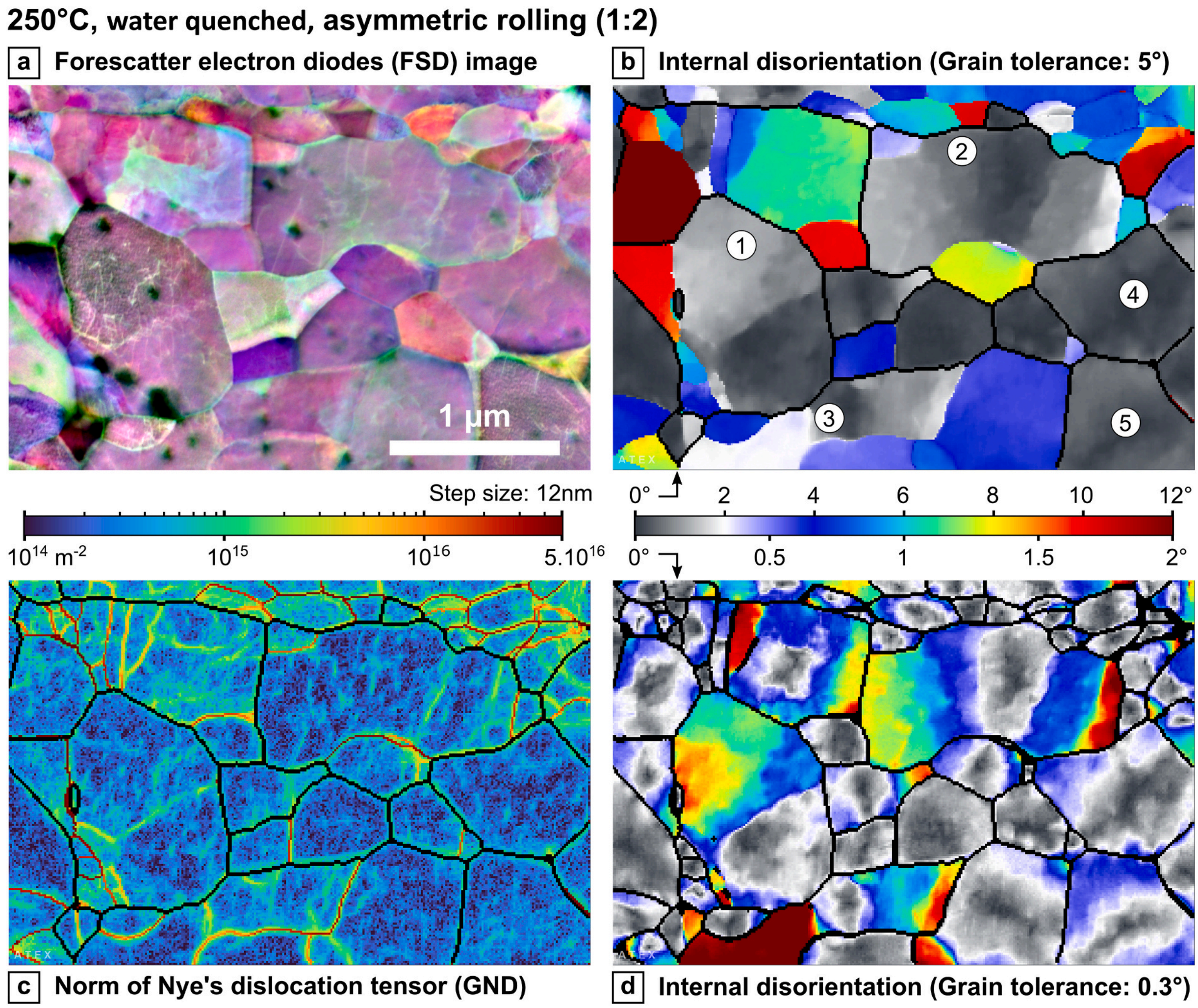

Fig. 13. HR-TKD analysis of sample rolled with roll diameters ratio 1:2 at 250 °C temperature and water quenched. (a) FSD image. (b) Internal disorientation angle of grains defined with a tolerance angle of 5°. (c) GND densities associated to (b). (d) Internal disorientation angle of grains defined with a tolerance angle of 0.3° after re-indexing.

Temperature about 450 °C is a low temperature for the ferritic steel to form fine grains at the grain boundaries of elongated grains in a classical neckless style (Fig. 5a). These formed grains in a classical neckless style does not require further analysis to be attributed to discontinuous type dynamic recrystallization. However, few sites of dynamic recrystallization were also along deformation and shear bands within the elongated bands of original grains. Due to having fewer sites of dynamic recrystallized grains within elongated grains, 450 °C could be the upper cut-off of continuous dynamic recrystallization. The examination of symmetric rolled samples at 600C, 450C and 250 °C in Figs. 4b and 6b suggests the reduction in flow stress by showing decreased number of in-grain shear bending at 450 °C as compared to 250 °C (or the flow stress at 250 °C) [27,30,40]. There are no in-grain shear bending at 600 °C which also means that the grains are yet to soften completely at 450 °C. Under this state, texture rotation by imposed asymmetry probably not only increase instabilities at the serrated boundaries of elongated original grains (which are already under compression due to rolling strain) but can also assists in forming shear bands and microbands within the elongated grains. The shear bands can have both ±35° inclination to the rolling direction, which also means a possible continuity of their formation or still being remained at 450 °C with imposed shear strain. That is why a transition state of dynamic recrystallization from continuous to discontinuous type is observed at 450 °C.

These dynamically recrystallized grains, marked in Fig. 12b (450 °C), are smaller and have more substructural features than at higher temperatures. The HR-TKD measurement of the GND densities especially shows it (Fig. 12c). In fact, the GND densities contained in these grains show remarkable difference, both in terms of increased GND value within internal core of the grains and near their substructures also if compared to the 700 °C. The dynamically recrystallized grains present disorientation profile within 2° (Fig. 12d). But, some of the grains have strong intensity profile as well (grains #2, 3 and 4), which can also mean a tendency to be under subdivision process. From their morphology point of view, they are less faceted. The dynamically recrystallized grains are in state of bulging out from their surrounding grains to grow and become more equiaxed type. For example, the dotted line in Fig. 12b highlights such type of a grain, which is forming neckless type of structure with its surrounding neighbors. Thereby, HR-TKD analysis validates having more discontinuous than the continuous type of dynamic recrystallization at 450 °C.

With further decrease in temperature to 250 °C, in-grain shear band formation becomes intense as compared to 450 °C and even room temperature [27,40]. It is due to lying in the temperature range of dynamic strain aging effect, thus the equiaxed grain formation will be affected by increased flow stress and in-grain shear bands. Temperature is indeed not so high, which is also responsible for the activation of grain fragmentation process to form more fragmented and equiaxed type

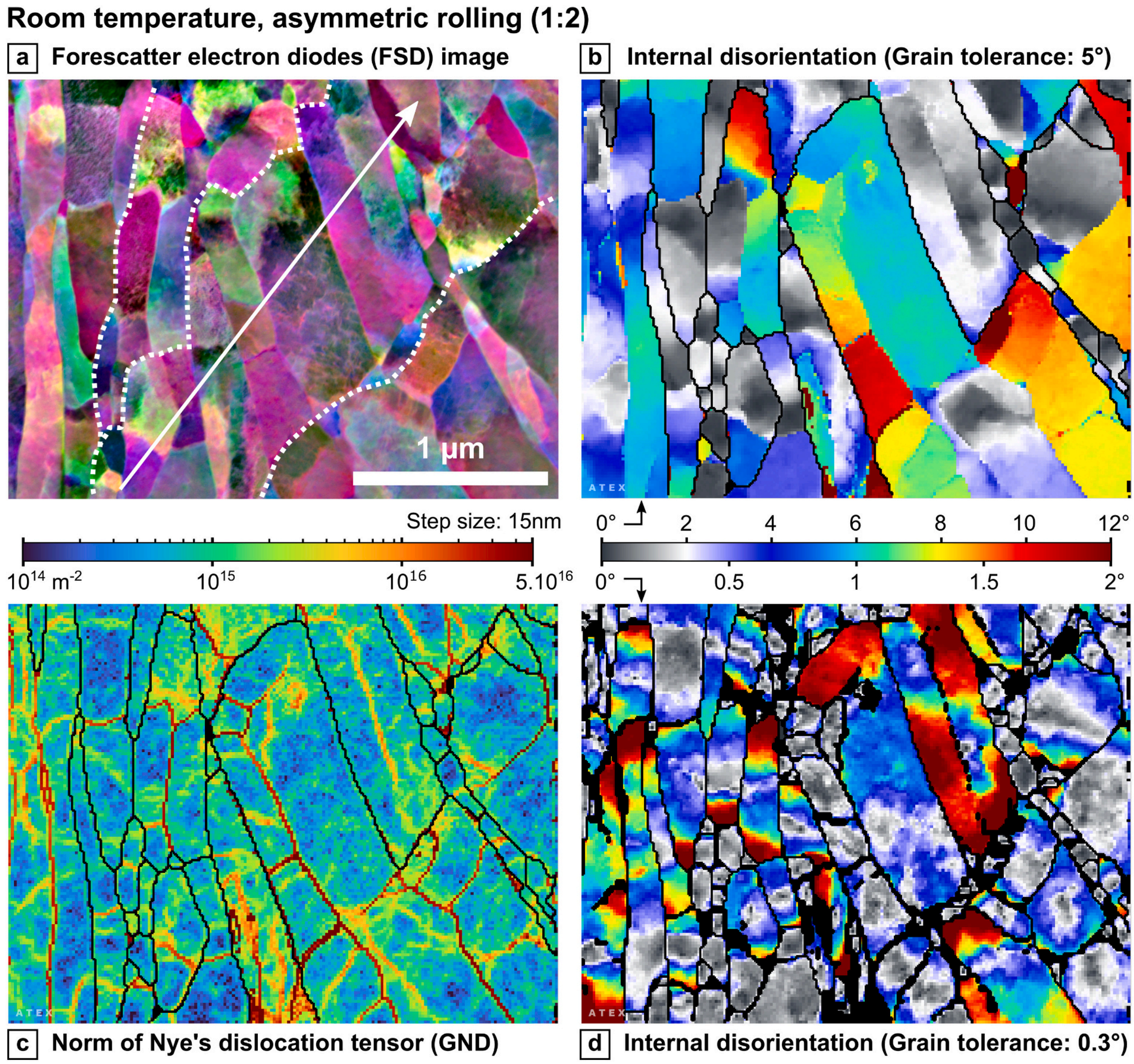

Fig. 14. HR-TKD analysis of sample rolled with roll diameters ratio 1:2 at room temperature. (a) FSD image. (b) Internal disorientation angle of grains defined with a tolerance angle of 5°. (c) GND densities associated to (b). (d) Internal disorientation angle of grains defined with a tolerance angle of 0.3° after re-indexing.

grains. In accord to it, the conventional EBSD map at 250 °C (Fig. 5b) has higher fraction of fragmented and equiaxed grains than at 450 °C and room temperature (Figs. 5a, 7a). The characteristic of these grains by HR-TKD analysis shows being under grain subdivision/fragmentation process where grains are towards forming equiaxed shape but also show having ellipticity as well (as marked in Fig. 13b). These fine grains show increased intensity spread of internal disorientation within 2° (Fig. 13d) and also more substructures (Fig. 13c) than what was observed at 450 °C. It is the low temperature and strained condition which leads to term these grains formed by continuous type of dynamic recrystallization.

The characteristic of fine grains formed by the fragmentation at room temperature is similar to that at 250 °C. From Fig. 7a, it was noticed that recrystallized grains are fine and having more elliptical shape than the equiaxed (see close-up). At this temperature, HR-TKD measurements were carried out on a deformation band which was branching out from another elongated grain, as indicated in white in the FSD image (Fig. 14a). So, it was expected to have more fragmented and equiaxed grains in this region enclosed with high angle boundaries. Instead, they present high grain internal disorientation (Fig. 14b, d) and substructures (Fig. 14c). It is due to the grain fragmentation process which is solely responsible for their formation at room temperature. Thereby, formed grains tend to have higher grain internal disorientation and substructures than what was noticed with temperature assistance. Surely, it is a continuous dynamic recrystallization but applied strain in a single pass rolling is not so high as it occurs in other severe plastic deformation methods. Therefore, it also leads to have fragmented yet elongated grains along with fine equiaxed grains. In fact, the tendency of these grains to have increased internal disorientation distribution within them as well as at their peripheral front with neighboring grains is clearly noticed.

5. Conclusions

The connection between dynamic recrystallization and texture or vice versa in warm temperature range of rolling was studied on extra low carbon steel. The effectiveness of applied strain path in rolling increased by changing the ratios of roll diameters from 1:1 to 1:2. The response of deformed microstructure with imposed shear on plane strain compression condition is significant. From this study, the following conclusions are drawn when symmetric rolling is compared with asymmetric rolling of the roll diameters ratio of 1:2.

1. Dynamic recovery prevails in deformed microstructures of warm symmetric rolling from 700 °C to room temperature but discontinuous dynamic recrystallization also apparently occurs at 600 °C and above. These so-formed grains are very fine and sparsely distributed along the grain boundaries.
2. The degree of rolling texture rotation and associated increase in geometrically necessary dislocations are responsible for the noticeable change in deformed microstructure when asymmetric conditions are imposed in rolling.
3. Increased flow stress at 250 °C due to dynamic strain aging leads to increase in-grain shear bands in symmetric rolling whereas grain fragmentation increases, and texture intensity weaken in the asymmetric case.
4. 450 °C lies in the temperature range where grains are softer and also have in-grain shear bands which leads them to transit from continuous dynamic recrystallization to discontinuous dynamic recrystallization by forming classical necklace of recrystallized grains at the original grain boundaries.
5. At 600 °C, increased grain softening leads to increased fraction of discontinuous dynamic recrystallization in asymmetric cases whereas absences of in-grain shear bands in symmetric rolling.
6. High-angular resolution on-axis TKD analyses allowed to reveal that a dynamically recrystallized grain possesses internal disorientation distribution profile bellow 2° and eventually sub grain boundaries (GND). All of which increases as the warm rolling temperature decreases.

Funding

This research did not receive any specific grant from funding agencies in public, commercial or not-for-profit sectors.

Data availability

The supporting data of this study are available from the corresponding author upon request.

CRediT authorship contribution statement

Satyaveer Singh Dhinwal: Conceptualization, Methodology, Validation, Formal analysis, Investigation, Writing – original draft, Writing – review & editing, Visualization. **Clément Ernould:** Methodology, Validation, Formal analysis, Investigation, Writing – review & editing, Visualization. **Benoît Beausir:** Validation, Writing – review & editing, Supervision.

Declaration of Competing Interest

The authors declare that they have no known competing financial interests or personal relationships that could have appeared to influence the work reported in this paper.

Acknowledgments

The authors gratefully acknowledge Surya N. Kumaran at LEM3 of Université de Lorraine, France to assist in the acquisition of EBSD maps for the overall texture measurements on large area of a specimen.

Appendix A. Bulk texture measurement for the asymmetric rolling with roll diameters ratio 1:2 between room temperature and 600 °C

The bulk texture measurements were carried out by using both X-ray diffraction and Electron Back Scattered Diffraction (EBSD). For X-ray diffraction, the irradiated surface area of sample was 30 mm × 30 mm. This surface area was taken from the mid thickness region, which lies perpendicular to the normal direction of a rolled sheet with 75% thickness reduction in a pass. Both defocus and background corrections were applied to obtain Orientation Distribution Function (ODF) from three measured raw pole figures {110}. {200} and {112} for the extra-low carbon grade of ferritic steels. The relevancy of the Fig. A below obtained from X-ray diffraction is to the overall texture intensity measured from the Electron Back Scattered Diffraction (EBSD) in Figs. 8 and 9. An area of 3 mm in length and 0.5 mm in height was scanned to achieve a convincing statistics by using EBSD. A representative EBSD map size for the bulk texture is shown below in figure (a). It is clear now that both EBSD and X-ray diffraction represent the same trend in overall texture intensity with increase in temperature thus the analysis related to texture formed by the dynamically recrystallized grains in Figs. 8,9 and 10.

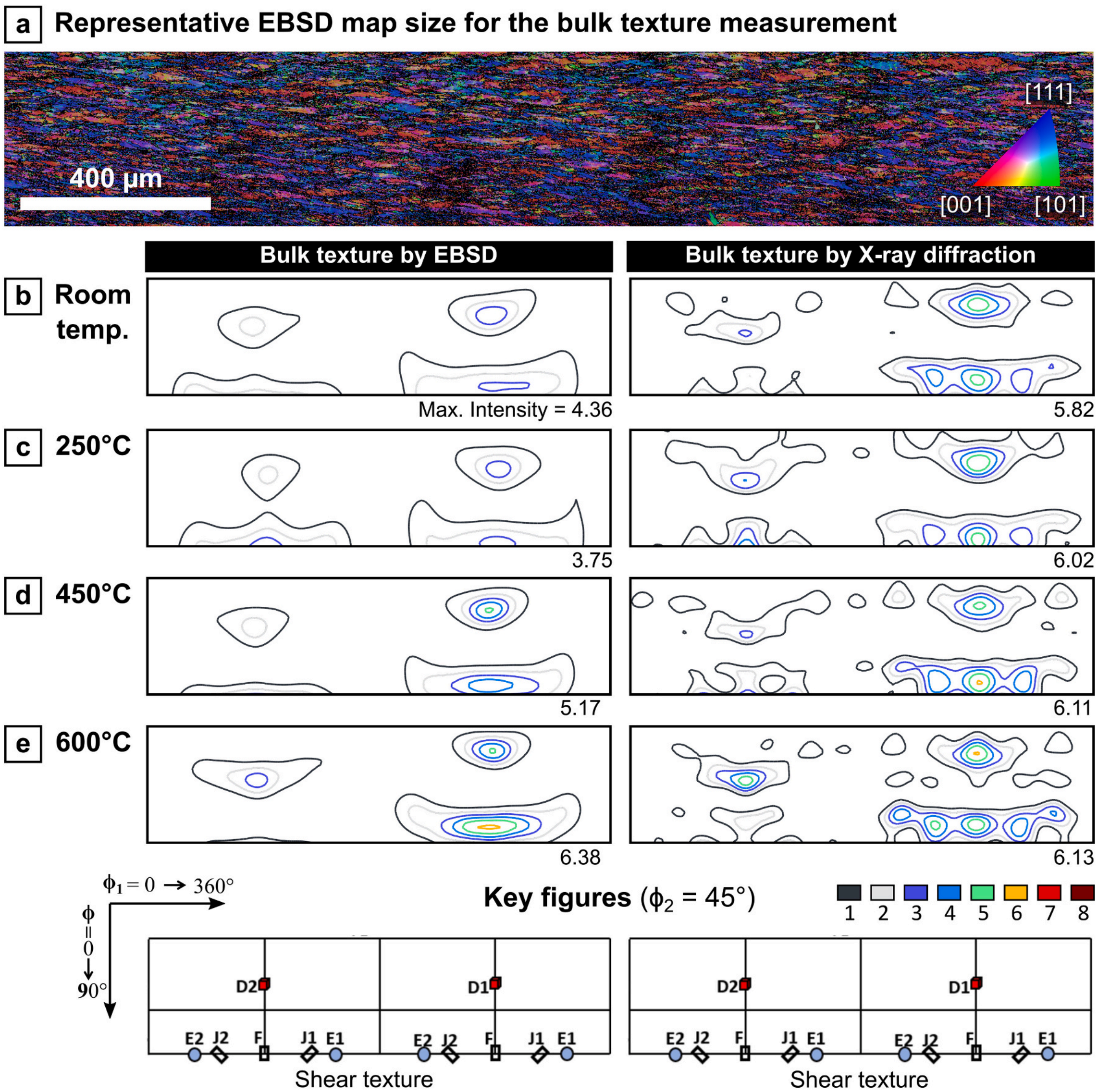

Fig. A.

Appendix B. Automatic detection of subgrain boundaries from HR-TKD measurements

Fig. B below re-uses the dataset of Fig. 14 (sample rolled with roll diameters ratio 1:2 at room temperature) to illustrate how to detect disorientation angle distribution within the subgrains (see Figs. 11–14d) from HR-TKD measurements and why it was required in the present investigation.

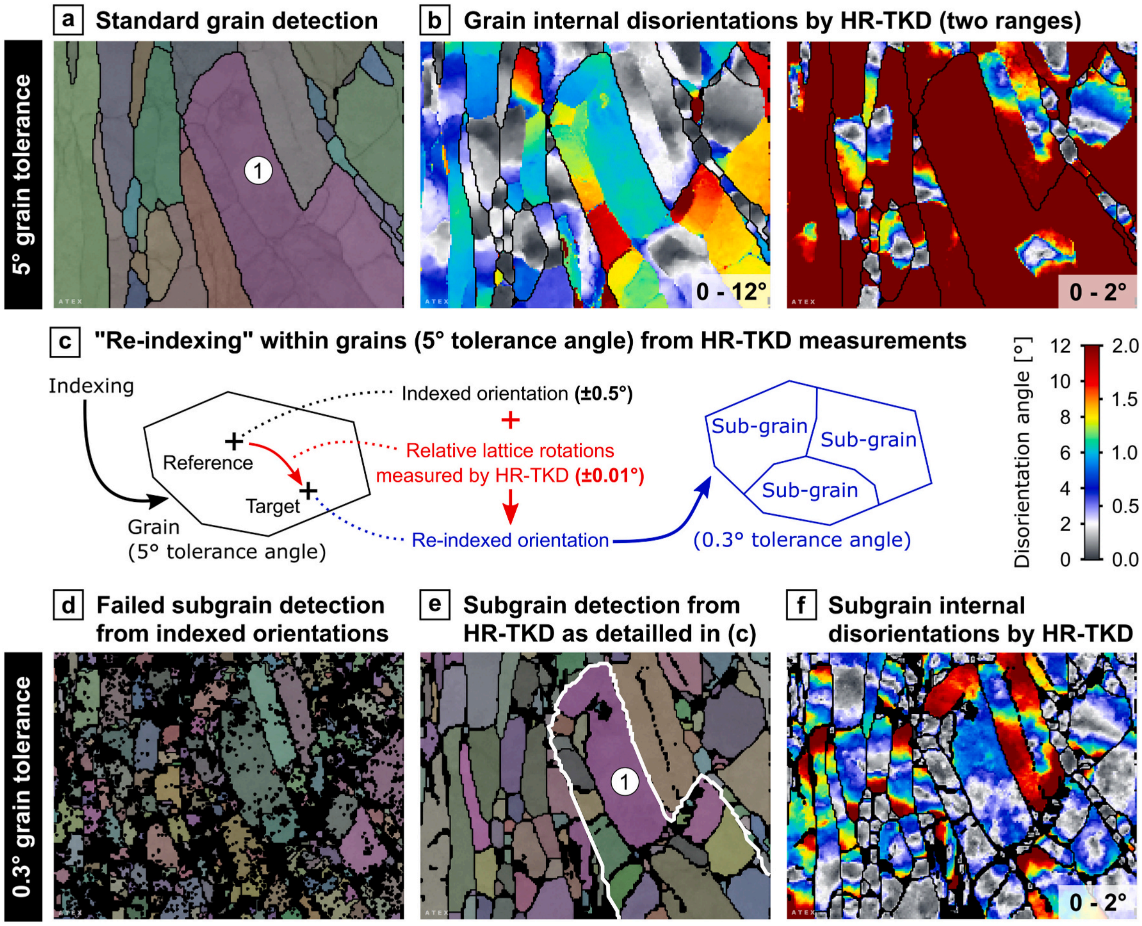

Fig. B.

To present internal disorientation distribution maps, the prime task is to detect grains with the usual tolerance angle of 5°, like in Fig. Ba, where each grain assigned with a different color. Within each grain, a point is then taken as a reference and the relative lattice rotations between the latter and any other target points belonging to this grain were accurately measured by HR-TKD (Typical resolution is 0.01) [63]. Such measurement highlights the presence of subgrains having internal disorientation in the range of 0 to 12° or more within the detected grains of 5° tolerance angle. Although, in map like Fig. Bb (left), the grains which are dynamically recrystallized or in such formation process can be identified by having internal disorientation between 0 and 2°. However, further insights such as a distribution profile of internal disorientation within the range of 0 to 2° is one of the perquisite criteria to discuss about the dynamic recrystallization.

By reducing the plotted angular range of internal disorientation between 0 and 2°, one can observe distribution profile within the dynamically recrystallized grains and also in the segments of those grains which are in the process of such formation (right side of Fig. Bb). From dynamic recrystallized grain criteria point of view, such an observation qualifies them to be called dynamic recrystallized grain or in the process of forming. However, reducing the angular range between 0 and 2° also simply saturates the most of map area (right side of Fig. Bb). In this way, the acquired knowledge related to the internal disorientation vanishes within subgrains of those grains which were still in deformed or partially dynamic recrystallized state. Thereby 5° grain tolerance angle should reduce to the subgrain scale. By this way, the internal disorientations profile not only presented within dynamic recrystallized grains or in the process of forming but also within subgrains of a grain. Such map will be a complementary to the maps in Fig. Ba and b for the comprehensive understanding.

A direct subgrain detection from standard Hough-transformed based indexing fails as it leads to many irrelevant “grains” of less than ten pixels (in black) in Fig. Bd. Indeed, the grain tolerance of 0.3° is below the typical Hough-transform based indexing uncertainty on orientations (0.5°). However, it is known now that the HR-TKD makes fine observation of disorientations less than of 1° missed by the standard Hough-transformed based indexing [63]. Therefore, a scheme proposed in Fig. Bc to fairly detects subgrains. Here, the target points are re-indexed knowing the relative lattice rotations measured by HR-TKD and the indexed orientation of the reference point to detect the subgrains. Fig. Be presents detected subgrains which were concealed in Fig. Ba. For example grain numbered #1 in Fig. Ba and Be. The 0.3° grain tolerance angle was determined empirically by steadily decreasing it from 5° (no claim to be optimized nor unfailing). Although seemingly low, this threshold is applied to the neighboring pixels of TKD maps having a 10 to 20 nm step size. Nevertheless, a slightly higher tolerances such as 0.8–1° misses many subgrain boundaries.

Finally, the subgrain internal disorientation angle distribution was derived from the re-indexed orientation and presented in Fig. Bf. The Fig. Bf also has the same angular resolution as in Fig. Bb but they differ on the basis of reference point selection within a defined grain. It also explains the observed difference in the profile of internal disorientation angle distribution between Fig. Bf and the unsaturated regions in the right side of Fig. Bb.

References

[1] J.J. Jonas, Dynamic recrystallization—scientific curiosity or industrial tool? Mater. Sci. Eng. A 184 (1994) 155–165, https://doi.org/10.1016/0921-5093(94)91028-6.

[2] N.D. Stepanov, D.G. Shaysultanov, N.Y. Yurchenko, S.V. Zherebtsov, A.N. Ladygin, G.A. Salishchev, M.A. Tikhonovsky, High temperature deformation behavior and dynamic recrystallization in CoCrFeNiMn high entropy alloy, Mater. Sci. Eng. A 636 (2015) 188–195, https://doi.org/10.1016/j.msea.2015.03.097.

[3] R.R. Eleti, A.H. Chokshi, A. Shibata, N. Tsuji, Unique high-temperature deformation dominated by grain boundary sliding in heterogeneous necklace structure formed by dynamic recrystallization in HfNbTaTiZr BCC refractory high entropy alloy, Acta Mater. 183 (2020) 64–77, https://doi.org/10.1016/j.actamat.2019.11.001.

[4] N. Haghdadi, S. Primig, M. Annasamy, P. Cizek, P.D. Hodgson, D.M. Fabijanic, Dynamic recrystallization in AlXCoCrFeNi duplex high entropy alloys, J. Alloys Compd. 830 (2020), 154720, https://doi.org/10.1016/j.jallcom.2020.154720.

[5] J.J. Jonas, C.M. Sellars, W.J.M. Tegart, Strength and structure under hot-working conditions, Metall. Rev. 14 (1969) 1–24, https://doi.org/10.1179/mtlr.1969.14.1.1.

[6] R.A.P. Djaic, J.J. Jonas, Recrystallization of high carbon steel between intervals of high temperature deformation, Metall. Trans. A. 4 (1973) 621–624, https://doi.org/10.1007/bf02648720.

[7] E.I. Poliak, J.J. Jonas, Critical strain for dynamic recrystallization in variable strain rate hot deformation, ISIJ Int. 43 (2003) 692–700, https://doi.org/10.2355/isijinternational.43.692.

[8] H.J. McQueen, Development of dynamic recrystallization theory, Mater. Sci. Eng. A 387–389 (2004) 203–208, https://doi.org/10.1016/j.msea.2004.01.064.

[9] A. Dehghan-Manshadi, M.R. Barnett, P.D. Hodgson, Hot deformation and recrystallization of austenitic stainless steel: part I. dynamic recrystallization, Metall. Mater. Trans. A. 39 (2008) 1359–1370, https://doi.org/10.1007/s11661-008-9512-7.

[10] F. Chen, H. Zhu, W. Chen, H. Ou, Z. Cui, Multiscale modeling of discontinuous dynamic recrystallization during hot working by coupling multilevel cellular automaton and finite element method, Int. J. Plast. 145 (2021), 103064, https://doi.org/10.1016/j.ijplas.2021.103064.

[11] K. Huang, R.E. Logé, A review of dynamic recrystallization phenomena in metallic materials, Mater. Des. 111 (2016) 548–574, https://doi.org/10.1016/j.matdes.2016.09.012.

[12] S.I. Kim, S.H. Choi, Y. Lee, Influence of phosphorous and boron on dynamic recrystallization and microstructures of hot-rolled interstitial free steel, Mater. Sci. Eng. A 406 (2005) 125–133, https://doi.org/10.1016/j.msea.2005.06.040.

[13] T. Sakai, A. Belyakov, R. Kaibyshev, H. Miura, J.J. Jonas, Dynamic and post-dynamic recrystallization under hot, cold and severe plastic deformation conditions, Prog. Mater. Sci. 60 (2014) 130–207, https://doi.org/10.1016/j.pmatsci.2013.09.002.

[14] R.A. Petkovic, M.J. Luton, J.J. Jonas, Recovery and recrystallization of polycrystalline copper after hot working, Acta Metall. 27 (1979) 1633–1648, https://doi.org/10.1016/0001-6160(79)90045-2.

[15] H.J. Mcqueen, J.J. Jonas, Recovery and recrystallization during high temperature deformation, in: in: R.J.B.T.-T. on M.S.& T. ARSENAULT (Ed.), Plast. Deform. Mater, Elsevier, 1975, pp. 393–493, https://doi.org/10.1016/B978-0-12-341806-7.50014-3.

[16] C.M. Sellars, J.A. Whiteman, Recrystallization and grain growth in hot rolling, Met. Sci. 13 (1979) 187–194, https://doi.org/10.1179/msc.1979.13.3-4.187.

[17] W. Roberts, H. Boden, B. Ahlblom, Dynamic recrystallization kinetics, Met. Sci. 13 (1979) 195–205, https://doi.org/10.1179/msc.1979.13.3-4.195.

[18] T. Sakai, J.J. Jonas, Overview no., 35 dynamic recrystallization: mechanical and microstructural considerations, Acta Metall. 32 (1984) 189–209, https://doi.org/10.1016/0001-6160(84)90049-X.

[19] R.A. Petković, M.J. Luton, J.J. Jonas, Recovery and recrystallization of carbon steel between intervals of hot working, Can. Metall. Q. 14 (1975) 137–145, https://doi.org/10.1179/000844375795050201.

[20] A. Hildenbrand, L.S. Tóth, A. Molinari, J. Baczynski, J.J. Jonas, Self-consistent polycrystal modelling of dynamic recrystallization during the shear deformation of a Ti if steel, Acta Mater. 47 (1999) 447–460, https://doi.org/10.1016/S1359-6454(98)00384-X.

[21] S.H. Cho, K.B. Kang, J.J. Jonas, Dynamic, static and metadynamic recrystallization of a Nb-microalloyed steel, ISIJ Int. 41 (2001) 63–69, https://doi.org/10.2355/isijinternational.41.63.

[22] W. Blum, Q. Zhu, R. Merkel, H.J. McQueen, Geometric dynamic recrystallization in hot torsion of Al-5Mg-0.6Mn (AA5083), Mater. Sci. Eng. A 205 (1996) 23–30, https://doi.org/10.1016/0921-5093(95)09990-5.

[23] M.E. Kassner, S.R. Barrabes, New developments in geometric dynamic recrystallization, Mater. Sci. Eng. A 410–411 (2005) 152–155, https://doi.org/10.1016/j.msea.2005.08.052.

[24] A. Najafi-Zadeh, J.J. Jonas, S. Yue, Grain refinement by dynamic recrystallization during the simulated warm-rolling of interstitial free steels, Metall. Trans. A. 23 (1992) 2607–2617, https://doi.org/10.1007/BF02658064.

[25] G.H. Akbari, C.M. Sellars, J.A. Whiteman, Microstructural development during warm rolling of an if steel, Acta Mater. 45 (1997) 5047–5058, https://doi.org/10.1016/S1359-6454(97)00170-5.

[26] N. Tsuji, Y. Matsubara, Y. Saito, Dynamic recrystallization of ferrite in interstitial free steel, Scr. Mater. 37 (1997) 477–484, https://doi.org/10.1016/S1359-6462(97)00123-1.

[27] M.R. Barnett, J.J. Jonas, Distinctive aspects of the physical metallurgy of warm rolling, ISIJ Int. 39 (1999) 856–873, https://doi.org/10.2355/isijinternational.39.856.

[28] B. Eghbali, A. Abdollah-zadeh, P.D. Hodgson, Dynamic softening of ferrite during large strain warm deformation of a plain-carbon steel, Mater. Sci. Eng. A 462 (2007) 259–263, https://doi.org/10.1016/j.msea.2006.04.154.

[29] A.O. Humphreys, D. Liu, M.R. Toroghinejad, E. Essadiqi, J.J. Jonas, Warm rolling behaviour of low carbon steels, Mater. Sci. Technol. 19 (2003) 709–714, https://doi.org/10.1179/026708303225002848.

[30] J.J. Jonas, Effects of shear band formation on texture development in warm-rolled IF steels, J. Mater. Process. Technol. 117 (2001) 293–299, https://doi.org/10.1016/S0924-0136(01)00786-5.

[31] M.R. Toroghinejad, A.O. Humphreys, D. Liu, F. Ashrafizadeh, A. Najafizadeh, J. J. Jonas, Effect of rolling temperature on the deformation and recrystallization textures of warm-rolled steels, Metall. Mater. Trans. A Phys. Metall. Mater. Sci. 34 (A) (2003) 1163–1174, https://doi.org/10.1007/s11661-003-0136-7.

[32] C. Huang, E.B. Hawbolt, X. Chen, T.R. Meadowcroft, D.K. Matlock, Flow stress modeling and warm rolling simulation behavior of two Ti-Nb interstitial-free steels in the ferrite region, Acta Mater. 49 (2001) 1445–1452, https://doi.org/10.1016/S1359-6454(01)00032-5.

[33] A. Haldar, R.K. Ray, Microstructural and textural development in an extra low carbon steel during warm rolling, Mater. Sci. Eng. A 391 (2005) 402–407, https://doi.org/10.1016/j.msea.2004.09.014.

[34] B. Eghbali, M. Shaban, Warm deformation microstructure of a plain carbon steel, J. Iron Steel Res. Int. 18 (2011) 41–46, https://doi.org/10.1016/S1006-706X(11)60088-5.

[35] E.V. Pereloma, I.B. Timokhina, J.J. Jonas, M.K. Miller, Fine-scale microstructural investigations of warm rolled low-carbon steels with and without Cr, P, and B additions, Acta Mater. 54 (2006) 4539–4551, https://doi.org/10.1016/j.actamat.2006.05.040.

[36] A. Oudin, M.R. Barnett, P.D. Hodgson, Grain size effect on the warm deformation behaviour of a Ti-IF steel, Mater. Sci. Eng. A 367 (2004) 282–294, https://doi.org/10.1016/j.msea.2003.10.273.

[37] S.V.S.N. Murty, S. Torizuka, K. Nagai, T. Kitai, Y. Kogo, Dynamic recrystallization of ferrite during warm deformation of ultrafine grained ultra-low carbon steel, Scr. Mater. 53 (2005) 763–768, https://doi.org/10.1016/j.scriptamat.2005.05.027.

[38] S.V.S. Narayana Murty, S. Torizuka, K. Nagai, T. Kitai, Y. Kogo, Grain boundary diffusion controlled ultrafine grain formation during large strain-high Z deformation of coarse (200μm) grained ultra-low carbon steel, Mater. Sci. Eng. A 457 (2007) 162–168, https://doi.org/10.1016/j.msea.2006.12.078.

[39] I.P. Pinheiro, R. Barbosa, P.R. Cetlin, Effect of strain path on the dynamic restoration of interstitial free steel in the austenitic temperature range, Scr. Mater. 52 (2005) 639–644, https://doi.org/10.1016/j.scriptamat.2004.11.020.

[40] M.R. Barnett, J.J. Jonas, Influence of ferrite rolling temperature on microstructure and texture in deformed low C and IF steels, ISIJ Int. 37 (1997) 697–705, https://doi.org/10.2355/isijinternational.37.697.

[41] T. Öztürk, Deformation and recrystallization textures in cross-rolled sheets of copper and α-brass, Scr. Metall. 22 (1988) 1611–1616, https://doi.org/10.1016/S0036-9748(88)80252-7.

[42] A. Böcker, H. Klein, H. Bunge, Development of cross-rolling textures in ARMCOIRON, Text. Stress. Microstruct. 12 (1990) 103–123, https://doi.org/10.1155/TSM.12.103.

[43] A. Böcker, H. Klein, H.J. Bunge, Development of cross-rolling textures in AlMn1, Text. Microstruct. 12 (1990), 275912, https://doi.org/10.1155/TSM.12.155.

[44] N.P. Gurao, S. Sethuraman, S. Suwas, Effect of strain path change on the evolution of texture and microstructure during rolling of copper and nickel, Mater. Sci. Eng. A 528 (2011) 7739–7750, https://doi.org/10.1016/j.msea.2011.06.062.

[45] S.S. Dhinwal, L.S. Toth, Effect of strain path change on texture and microstructure evolution in asymmetric rolled extra-low carbon steel, Mater. Charact. 169 (2020), 110578, https://doi.org/10.1016/j.matchar.2020.110578.

[46] D. Pustovoytov, A. Pesin, P. Tandon, Asymmetric (Hot, warm, cold, cryo) rolling of light alloys: a review, Metals (Basel). 11 (2021) 1–46, https://doi.org/10.3390/met11060956.

[47] S.S. Dhinwal, L.S. Toth, P.D. Hodgson, A. Haldar, Effects of processing conditions on texture and microstructure evolution in extra-low carbon steel during multi-pass asymmetric rolling, Mater. 11 (2018), https://doi.org/10.3390/ma11081327.

[48] S.S. Dhinwal, L.S. Toth, Unlocking deformation path in asymmetric rolling by texture simulation, Mater. 13 (2020), https://doi.org/10.3390/ma13010101.

[49] S.S. Dhinwal, L.S. Toth, R. Lapovok, P.D. Hodgson, Tailoring one-pass asymmetric rolling of extra low carbon steel for shear texture and recrystallization, Materials (Basel). 12 (2019), https://doi.org/10.3390/ma12121935.

[50] S.H. Lee, D.N. Lee, Analysis of deformation textures of asymmetrically rolled steel sheets, Int. J. Mech. Sci. 43 (2001) 1997–2015, https://doi.org/10.1016/S0020-7403(01)00025-X.

[51] Y.G. Ko, J. Suharto, J.S. Lee, B.H. Park, D.H. Shin, Effect of roll speed ratio on deformation characteristics of IF steel subjected to differential speed rolling, Met. Mater. Int. 19 (2013) 603–609, https://doi.org/10.1007/s12540-013-3033-7.

[52] D. Orlov, A. Pougis, R. Lapovok, L.S. Toth, I.B. Timokhina, P.D. Hodgson, A. Haldar, D. Bhattacharjee, Asymmetric rolling of interstitial-free steel using differential roll diameters. Part I: mechanical properties and deformation textures, Metall. Mater. Trans. A. 44 (2013) 4346–4359, https://doi.org/10.1007/s11661-013-1791-y.

[53] R. Lapovok, D. Orlov, I.B. Timokhina, A. Pougis, L.S. Toth, P.D. Hodgson, A. Haldar, D. Bhattacharjee, Asymmetric rolling of interstitial-free steel using one idle roll, Metall. Mater. Trans. A. 43 (2012) 1328–1340, https://doi.org/10.1007/s11661-011-0960-0.

[54] L.S. Tóth, B. Beausir, D. Orlov, R. Lapovok, A. Haldar, Analysis of texture and R value variations in asymmetric rolling of IF steel, J. Mater. Process. Technol. 212 (2012) 509–515, https://doi.org/10.1016/j.jmatprotec.2011.10.018.
[55] D. Orlov, R. Lapovok, L.S. Toth, I.B. Timokhina, P.D. Hodgson, A. Haldar, D. Bhattacharjee, Asymmetric rolling of interstitial-free steel using differential roll diameters. Part II: microstructure and annealing effects, Metall. Mater. Trans. A. 45 (2014) 447–454, https://doi.org/10.1007/s11661-013-1958-6.
[56] M.H. Cai, S. Singh Dhinwal, Q.H. Han, Q. Chao, P.D. Hodgson, Gradient ultrafine ferrite and martensite structure and its tensile properties by asymmetric rolling in low carbon microalloyed steel, Mater. Sci. Eng. A 583 (2013) 205–209, https://doi.org/10.1016/j.msea.2013.06.076.
[57] F. Brasche, J. Wang, I. Timokhina, C. Haase, R. Lapovok, D.A. Molodov, Mechanical twinning and texture evolution during asymmetric warm rolling of a high manganese steel, Mater. Sci. Eng. A 764 (2019), 138183, https://doi.org/10.1016/j.msea.2019.138183.
[58] B. Beausir, S. Biswas, D.I. Kim, L.S. Tóth, S. Suwas, Analysis of microstructure and texture evolution in pure magnesium during symmetric and asymmetric rolling, Acta Mater. 57 (2009) 5061–5077, https://doi.org/10.1016/j.actamat.2009.07.008.
[59] A. Ohmori, S. Torizuka, K. Nagai, N. Koseki, Y. Kogo, Effect of deformation temperature and strain rate on evolution of ultrafine grained structure through single-pass large-strain warm deformation in a low carbon steel, Mater. Trans. 45 (2004) 2224–2231, https://doi.org/10.2320/matertrans.45.2224.
[60] J. Baczynski, J.J. Jonas, Torsion textures produced by dynamic recrystallization in α-iron and two interstitial-free steels, Metall. Mater. Trans. A. 29 (1998) 447–462, https://doi.org/10.1007/s11661-998-0125-y.
[61] B. Beausir, J.J. Fundenberger, Analysis Tools for Electron and X-Ray Diffraction, ATEX-Software, Www. Atex-Software. Eu, Univ. Lorraine-Metz, 2017.
[62] C. Ernould, B. Beausir, J.-J. Fundenberger, V. Taupin, E. Bouzy, Characterization at high spatial and angular resolutions of deformed nanostructures by on-axis HR-TKD, Scr. Mater. 185 (2020) 30–35, https://doi.org/10.1016/j.scriptamat.2020.04.005.
[63] C. Ernould, B. Beausir, J.-J. Fundenberger, V. Taupin, E. Bouzy, Global DIC approach guided by a cross-correlation based initial guess for HR-EBSD and on-axis HR-TKD, Acta Mater. 191 (2020) 131–148, https://doi.org/10.1016/j.actamat.2020.03.026.
[64] J.J. Fundenberger, E. Bouzy, D. Goran, J. Guyon, H. Yuan, A. Morawiec, Orientation mapping by transmission-SEM with an on-axis detector, Ultramicroscopy. 161 (2016) 17–22, https://doi.org/10.1016/j.ultramic.2015.11.002.
[65] H. Yuan, E. Brodu, C. Chen, E. Bouzy, J.-J. Fundenberger, L.S. Toth, On-axis versus off-axis transmission Kikuchi diffraction technique: application to the characterisation of severe plastic deformation-induced ultrafine-grained microstructures, J. Microsc. 267 (2017) 70–80, https://doi.org/10.1111/jmi.12548.
[66] Y. Shen, J. Xu, Y. Zhang, Y. Wang, J. Zhang, B. Yu, Y. Zeng, H. Miao, Spatial resolutions of on-Axis and off-Axis transmission Kikuchi diffraction methods, Appl. Sci. 9 (2019), https://doi.org/10.3390/app9214478.
[67] E. Brodu, E. Bouzy, Depth resolution dependence on sample thickness and incident energy in on-Axis transmission Kikuchi diffraction in scanning Electron microscope (SEM), Microsc. Microanal. 23 (2017) 1096–1106, doi:10.1017/S1431927617012697.
[68] R.G. Mariano, A. Yau, J.T. McKeown, M. Kumar, M.W. Kanan, Comparing scanning Electron microscope and transmission Electron microscope grain mapping techniques applied to well-defined and highly irregular nanoparticles, ACS Omega. 5 (2020) 2791–2799, https://doi.org/10.1021/acsomega.9b03505.
[69] C. Ernould, B. Beausir, J.-J. Fundenberger, V. Taupin, E. Bouzy, Integrated correction of optical distortions for global HR-EBSD techniques, Ultramicroscopy. 221 (2021), 113158, https://doi.org/10.1016/j.ultramic.2020.113158.
[70] G. Glover, C.M. Sellars, Recovery and recrystallization during high temperature deformation of α-iron, Metall. Trans. A. 4 (1973) 765–775, https://doi.org/10.1007/BF02643086.
[71] J.-H. Kang, S. Torizuka, Dynamic recrystallization by large strain deformation with a high strain rate in an ultralow carbon steel, Scr. Mater. 57 (2007) 1048–1051, https://doi.org/10.1016/j.scriptamat.2007.07.039.
[72] K. Kato, Y. Saito, T. Sakai, Investigation of recovery and recrystallization during hot rolling of stainless steels with high speed laboratory mill, Trans. Iron Steel Inst. Japan. 24 (1984) 1050–1054, https://doi.org/10.2355/isijinternational1966.24.1050.
[73] R. Gholizadeh, D. Terada, A. Shibata, N. Tsuji, Strain-dependence of deformation microstructures in ultra-low-C IF steel deformed to high strains by torsion at elevated temperatures, Nano, Mater. Sci. 2 (2020) 83–95, https://doi.org/10.1016/j.nanoms.2020.03.005.
[74] R. Gholizadeh, A. Shibata, N. Tsuji, Global view for grain refinement in ultra-low-C IF steel during high-strain deformation at various temperatures and strain rates, Materialia. 6 (2019), 100262, https://doi.org/10.1016/j.mtla.2019.100262.
[75] E.I. Poliak, J.J. Jonas, Initiation of dynamic recrystallization in constant strain rate hot deformation, ISIJ Int. 43 (2003) 684–691, https://doi.org/10.2355/isijinternational.43.684.
[76] A. Wauthier, H. Regle, J. Formigoni, G. Herman, The effects of asymmetrical cold rolling on kinetics, grain size and texture in IF steels, Mater. Charact. 60 (2009) 90–95, https://doi.org/10.1016/j.matchar.2008.07.004.
[77] T. Ungár, L.S. Tóth, J. Illy, I. Kovács, Dislocation structure and work hardening in polycrystalline ofhc copper rods deformed by torsion and tension, Acta Metall. 34 (1986) 1257–1267, https://doi.org/10.1016/0001-6160(86)90012-X.
[78] D.A. Hughes, N. Hansen, High angle boundaries formed by grain subdivision mechanisms, Acta Mater. 45 (1997) 3871–3886, https://doi.org/10.1016/S1359-6454(97)00027-X.
[79] C.F. Gu, L.S. Tóth, M. Arzaghi, C.H.J. Davies, Effect of strain path on grain refinement in severely plastically deformed copper, Scr. Mater. 64 (2011) 284–287, https://doi.org/10.1016/j.scriptamat.2010.10.002.
[80] H.J. Mcqueen, N.D. Ryan, E.V. Konopleva, X. Xia, Formation and Application of Grain boundary Serrations 34, 1995, pp. 219–229.
[81] T. Chauve, M. Montagnat, F. Barou, K. Hidas, A. Tommasi, D. Mainprice, Investigation of nucleation processes during dynamic recrystallization of ice using cryo-EBSD, Philos. Trans. R. Soc. A Math. Phys. Eng. Sci. 375 (2017), https://doi.org/10.1098/rsta.2015.0345.
[82] J. Liu, H. Chen, Nucleation and grain boundary evolution in dynamic recrystallization of 316LN steel during hot deformation, Front. Mater. 6 (2019) 1–8, https://doi.org/10.3389/fmats.2019.00209.
[83] H.W. Son, J.W. Lee, S.K. Hyun, Mechanism of grain boundary serration during hot deformation of AZ31 alloy: role of grain boundary dislocations and grain boundary sliding, Int. J. Plast. 125 (2020) 118–132, https://doi.org/10.1016/j.ijplas.2019.09.003.
[84] A.M. Wusatowska-Sarnek, H. Miura, T. Sakai, Nucleation and microtexture development under dynamic recrystallization of copper, Mater. Sci. Eng. A 323 (2002) 177–186, https://doi.org/10.1016/S0921-5093(01)01336-3.
[85] P. Peng, K. Zhang, J. She, A. Tang, J. Zhang, K. Song, Q. Yang, F. Pan, Role of second phases and grain boundaries on dynamic recrystallization behavior in ZK60 magnesium alloy, J. Alloys Compd. 861 (2021), 157958, https://doi.org/10.1016/j.jallcom.2020.157958.